A symmetric Galerkin BEM variational framework for multi-domain interface problems

Loukas F. Kallivokas [a,*], Tanjeet Juneja [a], Jacobo Bielak [b]

[a] *Department of Civil Engineering, The University of Texas at Austin, 1 University Station C1748, Austin, TX 78712, USA*
[b] *Department of Civil and Environmental Engineering, Carnegie Mellon University, Pittsburgh, PA 15213, USA*

Abstract

In this paper we discuss an energy-based variational framework for the solution of interior problems in multiply-connected domains comprising multiple piecewise homogeneous subdomains, using exclusively boundary integral equations. The primary goal is to provide a unified variational setting that lends itself naturally to symmetric Galerkin boundary element formulations in terms of Dirichlet-type variables only.

The approach hinges on the explicit imposition of the normal derivative of the classical integral representation of the interior solution on each subdomain via Lagrange multipliers in the augmented Lagrangian of the system. We use Maue-type identities to resolve the hypersingular kernels, leading to a scheme that requires only standard single- and double-layer evaluations. In addition, the usual difficulty with multi-valued normals at subdomain corners is treated here within the same variational framework, by incorporating into the variational formulation the constraint equation between the limiting normal derivatives at either side of the corner. The resulting scheme remains fully symmetric.

The numerical implementation avoids the explicit presence of Neumann-type unknowns on the boundaries, through condensation at the subdomain level. In all integral evaluations, three- or four-point Gauss quadrature rules are sufficient for accurate results. We describe the theory and present illustrative examples for thermal and acoustic problems governed by Laplace and Helmholtz equations, respectively. This technique, however, can be applied without essential modification to more general problems.
© 2004 Published by Elsevier B.V.

Keywords: Material interfaces; Multi-domains; Boundary elements; Symmetric Galerkin BEM; Integral equations; Hypersingular kernels; Corner treatment

* Corresponding author. Fax: +1 512 471 7259.
E-mail addresses: loukas@mail.utexas.edu (L.F. Kallivokas), tjuneja@mail.utexas.edu (T. Juneja), jbielak@cmu.edu (J. Bielak).

1. Introduction

Boundary integral equations have been widely used for the solution of a variety of problems in engineering. The majority of published works have favored *ad-hoc* formulations based on reciprocity relations and collocation schemes for their numerical implementation. Though such formulations have provided robust solutions to engineering problems, the resulting discretized systems are typically dense and non-symmetric, thus entailing increased computational cost especially when compared to domain discretization methods. In the early nineties (with a few notable earlier exceptions (e.g. [1,2]), works based on both *ad-hoc* and systematic approaches have appeared, that typically lead to symmetric or near-symmetric formulations (see [3] for a fairly extensive recent review). Such approaches are presently referred to as symmetric Galerkin boundary element methods (SGBEM), for the majority of the published formulations are based on weighted residual techniques—thence the Galerkin designation—rather than on variational statements [3].

Multi-domain methods, or more appropriately, domain decomposition methods based exclusively on boundary elements have also appeared for both interior and exterior problems, e.g. [3–7]. The primary motivation for the multi-domain approaches for homogeneous domains stems from numerical considerations: by dividing up the original domain into smaller ones (termed macro-elements in e.g. [6]), and using Galerkin-type symmetric boundary element formulations, one arrives at symmetric block-sparse algebraic systems. The resulting systems of algebraic equations, though based on discretization of integral equations, highly resemble those resulting from domain finite elements.

Invariably, the SGBEM formulations in the majority of the published works result from a combination of the, so-called, hypersingular and regular boundary element methods, without the benefit of a systematic framework. Furthermore, as noted in [3], advances are lacking in the context of variational schemes (as opposed to reciprocity relations) on which to base the SGBEM formulations. Thus, in this paper we combine an energy-based variational statement with prior developments on domain decomposition schemes for the Helmholtz operator [4–6] to account for multi-zone problems, e.g., for problems where the material properties are different on each subdomain. We refer to such problems as interface problems. The primary ideas also follow earlier developments on the BEM variational formulations for elastostatics [7] and on the variational coupling of boundary and finite elements [2,8] and depart from the implementations based on Galerkin weighted-residual approaches (e.g. [9,10]). We also pay special attention to the solution near corners, and develop a scheme that completely eliminates the often-observed spurious oscillatory behavior in their vicinity. We remark that a symmetric collocation scheme is also recoverable from the proposed variational scheme, depending only on the approximation function choices (e.g. Dirac functions).

2. Mathematical development

To fix ideas we restrict the discussion to the interior acoustics problem in two dimensions where the primary variable is the acoustic fluid pressure, henceforth denoted by u. The approach, however, is quite general and applicable to a variety of other problems with minor modifications needed to account for the specifics of the governing operator. In this section we derive a variational principle valid for the prototype interface problem defined below.

2.1. Problem strong statement

Without loss of generality, we consider the following simple interface problem (Fig. 1): Let $\Omega \subset \Re^2$ represent a two-zone region, occupied by two separate, linear, inviscid, and compressible fluids, homogeneous within each sub-region; specifically, let $\Omega = \Omega_1 \cup \Omega_2$, where Ω_1 is occupied by an acoustic fluid with density
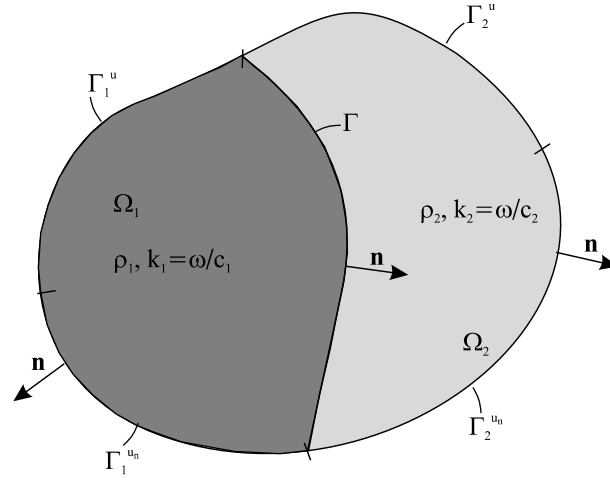
Fig. 1. Interface problem definition.

ρ_1 and characterized by a wave speed of c_1. Similarly, Ω_2's corresponding material characteristics are ρ_2 and c_2. Let $\partial\Omega_1$ and $\partial\Omega_2$ denote the closed boundaries of Ω_1 and Ω_2, respectively. Let Γ denote the common interface between Ω_1 and Ω_2, i.e., $\Gamma = \partial\Omega_1 \cap \partial\Omega_2$. Furthermore, let $\partial\Omega_1 = \Gamma \cup \Gamma_1^u \cup \Gamma_1^{u_n}$ and $\partial\Omega_2 = \Gamma \cup \Gamma_2^u \cup \Gamma_2^{u_n}$, where Γ_1^u and Γ_2^u denote the parts of $\partial\Omega_1$ and $\partial\Omega_2$ with prescribed Dirichlet data, and $\Gamma_1^{u_n}$ and $\Gamma_2^{u_n}$ denote the $\partial\Omega_1$ and $\partial\Omega_2$ boundaries with prescribed Neumann data, respectively. For well-posed problems: $\Gamma_1^u \cap \Gamma_1^{u_n} = \emptyset$, and $\Gamma_2^u \cap \Gamma_2^{u_n} = \emptyset$. Then, the strong form of the problem can be stated as follows (an $e^{i\omega t}$ term has been assumed throughout).

Find the fluid pressures $u_1(\boldsymbol{x})$ in Ω_1, and $u_2(\boldsymbol{x})$ in Ω_2 such that:

$$\Delta u_1(\boldsymbol{x}) + k_1^2 u_1(\boldsymbol{x}) = 0, \quad \boldsymbol{x} \in \Omega_1, \tag{1a}$$

$$\Delta u_2(\boldsymbol{x}) + k_2^2 u_2(\boldsymbol{x}) = 0, \quad \boldsymbol{x} \in \Omega_2, \tag{1b}$$

$$u_1(\boldsymbol{x}) = u_2(\boldsymbol{x}), \quad \boldsymbol{x} \in \Gamma, \tag{1c}$$

$$\frac{1}{\rho_1} u_{1_n}(\boldsymbol{x}) = \frac{1}{\rho_2} u_{2_n}(\boldsymbol{x}), \quad \boldsymbol{x} \in \Gamma, \tag{1d}$$

$$u_1(\boldsymbol{x}) = g_1(\boldsymbol{x}), \quad \boldsymbol{x} \in \Gamma_1^u, \tag{1e}$$

$$u_2(\boldsymbol{x}) = g_2(\boldsymbol{x}), \quad \boldsymbol{x} \in \Gamma_2^u, \tag{1f}$$

$$u_{1_n}(\boldsymbol{x}) = h_1(\boldsymbol{x}), \quad \boldsymbol{x} \in \Gamma_1^{u_n}, \tag{1g}$$

$$u_{2_n}(\boldsymbol{x}) = h_2(\boldsymbol{x}), \quad \boldsymbol{x} \in \Gamma_2^{u_n}. \tag{1h}$$

Here $\boldsymbol{n}$ denotes the outward normal to the various boundary segments (Fig. 1); (1a) and (1b) are Helmholtz equations that govern the fluid pressure within each subdomain; $k_1 = \omega/c_1$ and $k_2 = \omega/c_2$ denote wavenumbers. (1c) and (1d) are the continuity conditions on the common interface Γ; specifically, (1c) denotes the continuity of pressures, and (1d) the continuity of fluid accelerations across Γ. For a heat-conduction problem, (1c) and (1d) should be replaced by the continuity of temperature and heat fluxes, respectively, whereas

for an elasticity problem the corresponding conditions are the continuity of displacements and tractions. g_1 and g_2 are prescribed Dirichlet data, and h_1 and h_2 are prescribed Neumann data.

2.2. Problem variational statement

Following classical lines, in order to derive a variational statement corresponding to (1), we start by considering the Lagrangian of the two-fluid system. Accordingly, let T denote kinetic energy, V potential energy, and W the potential of the external sources. Then, the Lagrangian $\mathscr{L}$ of the system can be defined as:

$$\mathscr{L} = T - V - W = \frac{1}{2\rho_1\omega^2}\int_{\Omega_1}\nabla u_1\cdot\nabla u_1\,\mathrm{d}\Omega_1 - \frac{1}{2\rho_1 c_1^2}\int_{\Omega_1}u_1^2\,\mathrm{d}\Omega_1$$
$$+ \frac{1}{2\rho_2\omega^2}\int_{\Omega_2}\nabla u_2\cdot\nabla u_2\,\mathrm{d}\Omega_2 - \frac{1}{2\rho_2 c_2^2}\int_{\Omega_2}u_2^2\,\mathrm{d}\Omega_2 - \frac{1}{\rho_1\omega^2}\int_{\Gamma_1^{u_n}}h_1 u_1\,\mathrm{d}\Gamma_1^{u_n} - \frac{1}{\rho_2\omega^2}\int_{\Gamma_2^{u_n}}h_2 u_2\,\mathrm{d}\Gamma_2^{u_n}.$$

(2)

To show the equivalence between (2) and (1), the vanishing of the first variation of $\mathscr{L}$ must recover the governing partial differential equations (1a) and (1b), and the interface and boundary conditions (1c)–(1h). Similarly a solution u_1, u_2 must render $\mathscr{L}$ stationary. We show next that stationarity of $\mathscr{L}$ implies (1). Accordingly, after invoking the divergence theorem and collecting like-terms, the first variation of the Lagrangian $\mathscr{L}$ becomes:

$$\delta\mathscr{L} = \frac{1}{\rho_1\omega^2}\int_{\Gamma_1^{u_n}}\delta u_1(u_{1_n} - h_1)\,\mathrm{d}\Gamma_1^{u_n} + \frac{1}{\rho_2\omega^2}\int_{\Gamma_2^{u_n}}\delta u_2(u_{2_n} - h_2)\,\mathrm{d}\Gamma_2^{u_n} + \frac{1}{\rho_1\omega^2}\int_{\Gamma_1^{u}}\delta u_1 u_{1_n}\,\mathrm{d}\Gamma_1^{u}$$
$$+ \frac{1}{\rho_2\omega^2}\int_{\Gamma_2^{u}}\delta u_2 u_{2_n}\,\mathrm{d}\Gamma_2^{u} - \frac{1}{\rho_1\omega^2}\int_{\Omega_1}\delta u_1\big(\Delta u_1 + k_1^2 u_1\big)\,\mathrm{d}\Omega_1 - \frac{1}{\rho_2\omega^2}\int_{\Omega_2}\delta u_2\big(\Delta u_2 + k_2^2 u_2\big)\,\mathrm{d}\Omega_2$$
$$+ \frac{1}{\rho_1\omega^2}\int_{\Gamma}\delta u_1 u_{1_n}\,\mathrm{d}\Gamma - \frac{1}{\rho_2\omega^2}\int_{\Gamma}\delta u_2 u_{2_n}\,\mathrm{d}\Gamma = 0$$

(3)

for all admissible δu_1, δu_2, which are such that:

$$\delta u_1 = 0, \quad \delta u_2 = 0 \text{ on } \Gamma_1^u \text{ and } \Gamma_2^u, \text{ respectively, and,} \tag{4a}$$

$$\delta u_1 = \delta u_2 \quad \text{on } \Gamma, \tag{4b}$$

whilst u_1 and u_2 are required to satisfy the continuity condition (1c) and the essential conditions (1e) and (1f). Clearly, the first and second terms in (3) recover the Neumann conditions (1g) and (1h), respectively; the third and fourth terms in (3) vanish as per (4a), the fifth and sixth terms in (3) vanish if and only if the governing equations (1a) and (1b) hold, and the last two terms, with the (4b) proviso, enforce the continuity condition (1d). Thus, for sufficiently smooth functions, the vanishing of the variation of the standard Lagrangian functional defined in (2), based on energy arguments alone, is tantamount to the strong form (1).

2.3. Modified variational statement

Next, in order to cast the variational statement (3) in terms of boundary integral equations only, we revisit the Lagrangian defined in (2), use integration by parts and the divergence theorem, to arrive at:

5

$$\mathscr{L} = \frac{1}{2\rho_1\omega^2}\int_{\partial\Omega_1} u_1 u_{1_n}\,\mathrm{d}(\partial\Omega_1) + \frac{1}{2\rho_2\omega^2}\int_{\partial\Omega_2} u_2 u_{2_n}\,\mathrm{d}(\partial\Omega_2) - \frac{1}{2\rho_1\omega^2}\int_{\Omega_1} u_1\big(\Delta u_1 + k_1^2 u_1\big)\mathrm{d}\Omega_1$$
$$- \frac{1}{2\rho_2\omega^2}\int_{\Omega_2} u_2\big(\Delta u_2 + k_2^2 u_2\big)\mathrm{d}\Omega_2 - \frac{1}{\rho_1\omega^2}\int_{\Gamma_1^{u_n}} h_1 u_1\,\mathrm{d}\Gamma_1^{u_n} - \frac{1}{\rho_2\omega^2}\int_{\Gamma_2^{u_n}} h_2 u_2\,\mathrm{d}\Gamma_2^{u_n}. \tag{5}$$

Clearly, if (1a) and (1b) are satisfied, the third and fourth domain terms in (5) vanish. Here, in order to ensure that (1a) and (1b) are satisfied, we use the Helmholtz integral representation to replace the domain integrals in (5); we do so by imposing it explicitly in the Lagrangian (5) via Lagrange multipliers for each of the two subdomains. This process leads to a modified Lagrangian and a modified variational statement. To illustrate the steps, we first discuss the specifics of the integral representation for u_1 (the process is similar for u_2). Thus, if u_1 satisfies (1a), then it also satisfies the integral representations (for smooth boundaries): [1]

$$\mathfrak{u}_1 = \mathfrak{D}_1[u_1] - \mathfrak{S}_1[u_{1_n}] \quad \text{in } \Omega_1, \tag{6}$$

where $\mathfrak{S}_1$ and $\mathfrak{D}_1$ are the single- and double-layers defined for any smooth function q as:

$$\mathfrak{S}_1[q](\boldsymbol{x}) = \int_{\partial\Omega_1} q(\boldsymbol{y}) G(\boldsymbol{x},\boldsymbol{y})\,\mathrm{d}(\partial\Omega_1(\boldsymbol{y})), \quad \boldsymbol{x},\boldsymbol{y} \in \Omega_1, \tag{7a}$$

$$\mathfrak{D}_1[q](\boldsymbol{x}) = \int_{\partial\Omega_1} q(\boldsymbol{y})\frac{\partial G(\boldsymbol{x},\boldsymbol{y})}{\partial n_{\boldsymbol{y}}}\,\mathrm{d}(\partial\Omega_1(\boldsymbol{y})), \quad \boldsymbol{x},\boldsymbol{y} \in \Omega_1, \tag{7b}$$

and $G(z)$, with $z = |\boldsymbol{x} - \boldsymbol{y}|$, is the fundamental solution, or Green's function, for (1a) and (1b):

$$G(z) = \frac{i}{4}H_0^{(2)}(kz) \quad \text{in } \boldsymbol{R}^2. \tag{8}$$

Thus, $\mathfrak{u}_1$ in (6) automatically satisfies (1a); for smooth q and smooth boundary curves the following limit relations also hold:

$$\lim_{\Omega_1 \ni \boldsymbol{x} \to \boldsymbol{x} \in \partial\Omega_1} \mathfrak{S}_1[q](\boldsymbol{x}) = S_1[q](\boldsymbol{x}), \quad \text{or} \quad \mathfrak{S}_1[q] = S_1[q], \text{ on } \partial\Omega_1, \tag{9a}$$

$$\lim_{\Omega_1 \ni \boldsymbol{x} \to \boldsymbol{x} \in \partial\Omega_1} \mathfrak{D}_1[q](\boldsymbol{x}) = \frac{1}{2}q(\boldsymbol{x}) + D_1[q](\boldsymbol{x}), \quad \text{or} \quad \mathfrak{D}_1[q] = \frac{1}{2}q + D_1[q], \text{ on } \partial\Omega_1, \tag{9b}$$

$$\lim_{\Omega_1 \ni \boldsymbol{x} \to \boldsymbol{x} \in \partial\Omega_1} \frac{\partial}{\partial n_{\boldsymbol{y}}}\mathfrak{S}_1[q](\boldsymbol{x}) = -\frac{1}{2}q(\boldsymbol{x}) + N_1[q](\boldsymbol{x}), \quad \text{or} \quad \frac{\partial}{\partial n}\mathfrak{S}_1[q] = -\frac{1}{2}q + N_1[q], \text{ on } \partial\Omega_1, \tag{9c}$$

$$\lim_{\Omega_1 \ni \boldsymbol{x} \to \boldsymbol{x} \in \partial\Omega_1} \frac{\partial}{\partial n_{\boldsymbol{y}}}\mathfrak{D}_1[q](\boldsymbol{x}) = M_1[q](\boldsymbol{x}), \quad \text{or} \quad \frac{\partial}{\partial n}\mathfrak{D}_1[q] = M_1[q], \text{ on } \partial\Omega_1, \tag{9d}$$

in which

---

[1] Henceforth, we use Euler script letters (e.g. $\mathfrak{S}$) for domain representations of the layers, and roman letters (e.g. S) for their boundary counterparts; similarly for u.

$$S_1[q](x) = \int_{\partial\Omega_1} q(y)G(x,y)\,\mathrm{d}(\partial\Omega_1(y)), \quad x,y \in \partial\Omega_1, \tag{10a}$$

$$D_1[q](x) = \int_{\partial\Omega_1} q(y)\frac{\partial G(x,y)}{\partial n_y}\,\mathrm{d}(\partial\Omega_1(y)), \quad x,y \in \partial\Omega_1, \tag{10b}$$

$$N_1[q](x) = \int_{\partial\Omega_1} q(y)\frac{\partial G(x,y)}{\partial n_x}\,\mathrm{d}(\partial\Omega_1(y)), \quad x,y \in \partial\Omega_1, \tag{10c}$$

$$M_1[q](x) = \int_{\partial\Omega_1} q(y)\frac{\partial^2 G(x,y)}{\partial n_x \partial n_y}\,\mathrm{d}(\partial\Omega_1(y)), \quad x,y \in \partial\Omega_1. \tag{10d}$$

where S_1 and D_1 above denote the single- and double-layer operators respectively, N_1 denotes the adjoint of D_1, and M_1 is the hypersingular operator (similarly for $\partial\Omega_2$). From (6) and (9) it follows that:

$$\frac{1}{2}u_1 - D_1[u_1] + S_1[u_{1_n}] = 0, \quad \text{on } \partial\Omega_1, \tag{11a}$$

$$\frac{1}{2}u_{1_n} - M_1[u_1] + N_1[u_{1_n}] = 0, \quad \text{on } \partial\Omega_1. \tag{11b}$$

We remark that either (11a) or (11b) ensure that any $\mathfrak{u}_1$ defined by (6), in which u_1, u_{1_n} satisfy (11a) or (11b), will also satisfy the domain equation (1a). We further remark that (11a) is the standard integral representation for the Helmholtz equation in terms of the single- and double-layer operators, whereas (11b) involves the double-layer adjoint operator N and the hypersingular operator M. One can make use of either (11a) or (11b) to augment the Lagrangian in (5). Here we favor the use of (11b), which contains the hypersingular kernel. Upon discretization, (11b) entails the numerical inversion of the double-layer term (D_1). By contrast, the use of (11a) entails the inversion of the single-layer term (S_1); the latter approach was used in [7]. We prefer to invert the operator of the second-kind (D) over that of the first-kind (S) since the former leads to a better conditioned algebraic system.

2.4. SGBEM variational statement

Let λ_1 and λ_2 denote Lagrange multipliers; then the Lagrangian (5) is augmented by imposing (11b) and its $\partial\Omega_2$ counterpart via the Lagrange multipliers λ_1 and λ_2, respectively. The modified Lagrangian $\hat{\mathscr{L}}$ thus becomes:

$$\begin{aligned}
\hat{\mathscr{L}} = {} & \frac{1}{2\rho_1\omega^2}\int_{\partial\Omega_1} u_1 u_{1_n}\,\mathrm{d}(\partial\Omega_1) + \frac{1}{2\rho_2\omega^2}\int_{\partial\Omega_2} u_2 u_{2_n}\,\mathrm{d}(\partial\Omega_2) - \frac{1}{2\rho_1\omega^2}\int_{\partial\Omega_1} \lambda_1\left[\frac{1}{2}u_{1_n} - M_1[u_1] + N_1[u_{1_n}]\right]\mathrm{d}(\partial\Omega_1) \\
& - \frac{1}{2\rho_2\omega^2}\int_{\partial\Omega_2} \lambda_2\left[\frac{1}{2}u_{2_n} - M_2[u_2] + N_2[u_{2_n}]\right]\mathrm{d}(\partial\Omega_2) - \frac{1}{\rho_1\omega^2}\int_{\Gamma_1^{u_n}} h_1 u_1\,\mathrm{d}\Gamma_1^{u_n} - \frac{1}{\rho_2\omega^2}\int_{\Gamma_2^{u_n}} h_2 u_2\,\mathrm{d}\Gamma_2^{u_n}.
\end{aligned} \tag{12}$$

The augmented Lagrangian $\hat{\mathscr{L}}$ in (12) forms the basis for the variational statement of the interface problem. The first variation of $\hat{\mathscr{L}}$ yields:

ARTICLE IN PRESS

L.F. Kallivokas et al. / Comput. Methods Appl. Mech. Engrg. xxx (2004) xxx–xxx   7

$$\delta\hat{\mathscr{L}} = -\frac{1}{2\rho_1\omega^2}\int_{\partial\Omega_1}\delta\lambda_1\left(\frac{1}{2}u_{1_n} - M_1[u_1] + N_1[u_{1_n}]\right)d(\partial\Omega_1)$$

$$-\frac{1}{2\rho_2\omega^2}\int_{\partial\Omega_2}\delta\lambda_2\left(\frac{1}{2}u_{2_n} - M_2[u_2] + N_2[u_{2_n}]\right)d(\partial\Omega_2) + \frac{1}{2\rho_1\omega^2}\int_{\partial\Omega_1}\delta u_{1_n}\left(u_1 - \frac{1}{2}\lambda_1 - D_1[\lambda_1]\right)d(\partial\Omega_1)$$

$$+\frac{1}{2\rho_2\omega^2}\int_{\partial\Omega_2}\delta u_{2_n}\left(u_2 - \frac{1}{2}\lambda_2 - D_2[\lambda_2]\right)d(\partial\Omega_2) + \frac{1}{2\rho_1\omega^2}\int_{\partial\Omega_1}\delta u_1(u_{1_n} + M_1[\lambda_1])d(\partial\Omega_1)$$

$$+\frac{1}{2\rho_2\omega^2}\int_{\partial\Omega_2}\delta u_2(u_{2_n} + M_2[\lambda_2])d(\partial\Omega_2) - \frac{1}{\rho_1\omega^2}\int_{\Gamma_1^{u_n}}h_1\delta u_1\,d\Gamma_1^{u_n} - \frac{1}{\rho_2\omega^2}\int_{\Gamma_2^{u_n}}h_2\delta u_2\,d\Gamma_2^{u_n} = 0.$$

$$(13)$$

To derive (13) use was also made of the following symmetry relations, valid for any two smooth functions p and q:

$$\int_{\partial\Omega}S[p](\boldsymbol{x})q(\boldsymbol{x})\,d(\partial\Omega) = \int_{\partial\Omega}S[q](\boldsymbol{x})p(\boldsymbol{x})\,d(\partial\Omega), \quad \boldsymbol{x}\in\partial\Omega, \tag{14a}$$

$$\int_{\partial\Omega}D[p](\boldsymbol{x})q(\boldsymbol{x})\,d(\partial\Omega) = \int_{\partial\Omega}N[q](\boldsymbol{x})p(\boldsymbol{x})\,d(\partial\Omega), \quad \boldsymbol{x}\in\partial\Omega, \tag{14b}$$

$$\int_{\partial\Omega}M[p](\boldsymbol{x})q(\boldsymbol{x})\,d(\partial\Omega) = \int_{\partial\Omega}M[q](\boldsymbol{x})p(\boldsymbol{x})\,d(\partial\Omega), \quad \boldsymbol{x}\in\partial\Omega, \tag{14c}$$

that is, S and M are self-adjoint, and D and N are adjoints.

Eq. (13) is the basis for our variational formulation. This variation has to hold for admissible δu_1, δu_2, which satisfy the essential conditions (4). Notice that no restrictions are imposed on δu_{1_n}, δu_{2_n}, $\delta\lambda_1$, and $\delta\lambda_2$. It is this unrestricted variation that will later allow us to perform condensation at the subdomain level.

We now need to show that (13) is equivalent to the original problem (1). The first two lines of (13) readily yield:

$$\frac{1}{2}u_{1_n} - M_1[u_1] + N_1[u_{1_n}] = 0, \quad \text{on } \partial\Omega_1, \tag{15a}$$

$$\frac{1}{2}u_{2_n} - M_2[u_2] + N_2[u_{2_n}] = 0, \quad \text{on } \partial\Omega_2. \tag{15b}$$

These equations imply that (1a) and (1b) are satisfied. On the other hand, the third and fourth lines of (13) give:

$$u_1 = \frac{1}{2}\lambda_1 + D_1[\lambda_1], \quad \text{on } \partial\Omega_1, \tag{15c}$$

$$u_2 = \frac{1}{2}\lambda_2 + D_2[\lambda_2], \quad \text{on } \partial\Omega_2, \tag{15d}$$

which also imply that (1a) and (1b) are satisfied, provided we define $\mathfrak{u}_1 \in \Omega_1$ and $\mathfrak{u}_2 \in \Omega_2$ by:

$$\mathfrak{u}_1 = \mathfrak{D}_1[\lambda_1] \quad \text{in } \Omega_1 \Rightarrow \begin{cases} u_1 = \frac{1}{2}\lambda_1 + D_1[\lambda_1] & \text{on } \partial\Omega_1, \\ u_{1_n} = M_1[\lambda_1] & \text{on } \partial\Omega_1, \end{cases} \tag{16a}$$

$$\mathfrak{u}_2 = \mathfrak{D}_2[\lambda_2] \quad \text{in } \Omega_2 \Rightarrow \begin{cases} u_2 = \frac{1}{2}\lambda_2 + D_2[\lambda_2] & \text{on } \partial\Omega_2, \\ u_{2_n} = M_2[\lambda_2] & \text{on } \partial\Omega_2. \end{cases} \tag{16b}$$

From (16a) and (16b) it follows that the Lagrange multipliers λ_1 and λ_2 represent the densities of the layers $\mathfrak{D}_1$ and $\mathfrak{D}_2$.

Eqs. (16), combined with the last four terms of (13), recover the interface condition (1d) and the Neumann conditions (1g) and (1h). This can be seen from:

$$
\begin{aligned}
0 ={} & \frac{1}{2\rho_1\omega^2}\int_{\partial\Omega_1}\delta u_1(u_{1_n}+M_1[\lambda_1])\mathrm{d}(\partial\Omega_1)+\frac{1}{2\rho_2\omega^2}\int_{\partial\Omega_2}\delta u_2(u_{2_n}+M_2[\lambda_2])\mathrm{d}(\partial\Omega_2)\\
& -\frac{1}{\rho_1\omega^2}\int_{\Gamma_1^{u_n}}h_1\delta u_1\,\mathrm{d}\Gamma_1^{u_n}-\frac{1}{\rho_2\omega^2}\int_{\Gamma_2^{u_n}}h_2\delta u_2\,\mathrm{d}\Gamma_2^{u_n}\\
={} & \frac{1}{2\rho_1\omega^2}\int_{\Gamma_1^{u_n}}\delta u_1(u_{1_n}+M_1[\lambda_1])\mathrm{d}\Gamma_1^{u_n}+\frac{1}{2\rho_1\omega^2}\int_{\Gamma}\delta u_1(u_{1_n}+M_1[\lambda_1])\mathrm{d}\Gamma\\
& +\frac{1}{2\rho_2\omega^2}\int_{\Gamma_2^{u_n}}\delta u_2(u_{2_n}+M_2[\lambda_2])\mathrm{d}\Gamma_2^{u_n}-\frac{1}{2\rho_2\omega^2}\int_{\Gamma}\delta u_2(u_{2_n}+M_2[\lambda_2])\mathrm{d}\Gamma\\
& -\frac{1}{\rho_1\omega^2}\int_{\Gamma_1^{u_n}}h_1\delta u_1\,\mathrm{d}\Gamma_1^{u_n}-\frac{1}{\rho_2\omega^2}\int_{\Gamma_2^{u_n}}h_2\delta u_2\,\mathrm{d}\Gamma_2^{u_n}=\frac{1}{\rho_1\omega^2}\int_{\Gamma_1^{u_n}}\delta u_1(u_{1_n}-h_1)\mathrm{d}\Gamma_1^{u_n}\\
& +\frac{1}{\rho_2\omega^2}\int_{\Gamma_2^{u_n}}\delta u_2(u_{2_n}-h_2)\mathrm{d}\Gamma_2^{u_n}+\frac{1}{\rho_1\omega^2}\int_{\Gamma}\delta u_1 u_{1_n}\,\mathrm{d}\Gamma-\frac{1}{\rho_2\omega^2}\int_{\Gamma}\delta u_2 u_{2_n}\,\mathrm{d}\Gamma.
\end{aligned}
\tag{17}
$$

If we now require that (17) hold for all admissible variations δu_1 and δu_2, we observe that the Neumann conditions (1g) and (1h) as well as the interface condition (1d) are satisfied. Thus, we have shown that the vanishing of the first variation of the augmented Lagrangian (13) ensures that the strong form of the problem (1) will be satisfied. The converse can also be shown readily starting from (13), but is omitted here for brevity (see [5] for a similar derivation).

SGBEM variational principle. The preceding results can be stated succinctly as follows.

Variational principle. The pressures $\mathfrak{u}_1$ and $\mathfrak{u}_2$ defined by:

$$\mathfrak{u}_1=\mathfrak{D}_1[\lambda_1]\quad\text{in }\Omega_1,\tag{18a}$$

$$\mathfrak{u}_2=\mathfrak{D}_2[\lambda_2]\quad\text{in }\Omega_2,\tag{18b}$$

are the solutions to the strong form (1) if and only if the first variation (13) of the functional $\hat{\mathscr{L}}$ defined by (12) vanishes for arbitrary variations $\delta\lambda_1$, $\delta\lambda_2$, δu_{1_n}, δu_{2_n}, δu_1 and δu_2.

In (13), $\delta\lambda_1$, $\delta\lambda_2$, δu_{1_n}, δu_{2_n} can be varied independently, but δu_1 and δu_2 are subject to $\delta u_1=0$ on Γ_1^u, $\delta u_2=0$ on Γ_2^u, and $\delta u_1=\delta u_2$ on Γ.

2.5. Remarks

- The Neumann interface condition (1d) is satisfied naturally by the variational principle. This allows us to approximate the unknowns with standard finite elements (low-order, compactly-supported, polynomial approximations) with no restrictions across the interface. Furthermore, since, for example, λ_1 is coupled only to u_1 within Ω_1, and λ_2 to u_2 within Ω_2, λ_1 and λ_2 may be condensed, leaving u_1 and u_2 as the only unknowns.
- Due to the fully variational form (12), the resulting algebraic system obtained upon discretization will be automatically symmetric.
- The augmented Lagrangian (12) and its first variation (13) contain boundary integrals involving the hypersingular operator M. For the numerical evaluation of these integrals there is no need for any special treatment. We use Maue's identity [11] to replace M with the weakly-singular operator S. For example, over $\partial\Omega_1$, and for any two smooth functions p, q, there holds:

ARTICLE IN PRESS

L.F. Kallivokas et al. / Comput. Methods Appl. Mech. Engrg. xxx (2004) xxx–xxx 9

$$\int_{\partial\Omega_1} pM_1[q]\,\mathrm{d}(\partial\Omega_1) = k_1^2 \int_{\partial\Omega_1} S_1[q\boldsymbol{n}]\cdot(p\boldsymbol{n})\,\mathrm{d}(\partial\Omega_1) - \int_{\partial\Omega_1} S_1[\boldsymbol{n}\times\boldsymbol{\nabla}q]\cdot(\boldsymbol{n}\times\boldsymbol{\nabla}p)\,\mathrm{d}(\partial\Omega_1). \tag{19}$$

This is an important advantage of variational over collocation methods, which require special techniques for evaluating the integrals that involve explicitly the hypersingular operator M_α, $\alpha = 1,2$ (e.g. [12]).

3. Numerical implementation

3.1. Discrete form of the variational principle

To arrive at the discrete form of (13), we start by considering standard piecewise polynomial approximations for the primary unknowns and their respective variations. Accordingly, let:

$$u_1(\boldsymbol{x}) = \boldsymbol{\phi}_1^{\mathrm{T}}(\boldsymbol{x})\boldsymbol{u}_1, \ \boldsymbol{x}\in\partial\Omega_1, \quad u_2(\boldsymbol{x}) = \boldsymbol{\phi}_2^{\mathrm{T}}(\boldsymbol{x})\boldsymbol{u}_2, \ \boldsymbol{x}\in\partial\Omega_2, \tag{20a}$$

$$u_{1n}(\boldsymbol{x}) = \boldsymbol{\psi}_1^{\mathrm{T}}(\boldsymbol{x})\boldsymbol{u}_{1_n}, \ \boldsymbol{x}\in\partial\Omega_1, \quad u_{2n}(\boldsymbol{x}) = \boldsymbol{\psi}_2^{\mathrm{T}}(\boldsymbol{x})\boldsymbol{u}_{2_n}, \ \boldsymbol{x}\in\partial\Omega_2, \tag{20b}$$

$$\lambda_1(\boldsymbol{x}) = \boldsymbol{\chi}_1^{\mathrm{T}}(\boldsymbol{x})\boldsymbol{\lambda}_1, \ \boldsymbol{x}\in\partial\Omega_1, \quad \lambda_2(\boldsymbol{x}) = \boldsymbol{\chi}_2^{\mathrm{T}}(\boldsymbol{x})\boldsymbol{\lambda}_2, \ \boldsymbol{x}\in\partial\Omega_2, \tag{20c}$$

$$\delta u_1(\boldsymbol{x}) = \delta\boldsymbol{u}_1^{\mathrm{T}}\boldsymbol{\phi}_1(\boldsymbol{x}), \ \boldsymbol{x}\in\partial\Omega_1, \quad \delta u_2(\boldsymbol{x}) = \delta\boldsymbol{u}_2^{\mathrm{T}}\boldsymbol{\phi}_2(\boldsymbol{x}), \ \boldsymbol{x}\in\partial\Omega_2, \tag{20d}$$

$$\delta u_{1n}(\boldsymbol{x}) = \delta\boldsymbol{u}_{1_n}^{\mathrm{T}}\boldsymbol{\psi}_1(\boldsymbol{x}), \ \boldsymbol{x}\in\partial\Omega_1, \quad \delta u_{2n}(\boldsymbol{x}) = \delta\boldsymbol{u}_{2_n}^{\mathrm{T}}\boldsymbol{\psi}_2(\boldsymbol{x}), \ \boldsymbol{x}\in\partial\Omega_2, \tag{20e}$$

$$\delta\lambda_1(\boldsymbol{x}) = \delta\boldsymbol{\lambda}_1^{\mathrm{T}}\boldsymbol{\chi}_1(\boldsymbol{x}), \ \boldsymbol{x}\in\partial\Omega_1, \quad \delta\lambda_2(\boldsymbol{x}) = \delta\boldsymbol{\lambda}_2^{\mathrm{T}}\boldsymbol{\chi}_2(\boldsymbol{x}), \ \boldsymbol{x}\in\partial\Omega_2, \tag{20f}$$

where $\boldsymbol{\phi}_\alpha(\boldsymbol{x})$, $\boldsymbol{\psi}_\alpha(\boldsymbol{x})$ and $\boldsymbol{\chi}_\alpha(\boldsymbol{x})$, with $\alpha = 1,2$, represent basis functions and $\boldsymbol{u}_1$, $\boldsymbol{u}_2$, $\boldsymbol{u}_{1_n}$, $\boldsymbol{u}_{2_n}$, $\boldsymbol{\lambda}_1$, and $\boldsymbol{\lambda}_2$ are the vectors of nodal unknowns. Next, the introduction of Eqs. (20), into the variation of the augmented Lagrangian (13), yields:

$$\delta\hat{\mathscr{L}} = \delta\boldsymbol{u}_{1_n}^{\mathrm{T}}[A_1\boldsymbol{u}_1 - B_1\boldsymbol{\lambda}_1] + \delta\boldsymbol{u}_{2_n}^{\mathrm{T}}[A_2\boldsymbol{u}_2 - B_2\boldsymbol{\lambda}_2] - \delta\boldsymbol{\lambda}_1^{\mathrm{T}}\big[B_1^{\mathrm{T}}\boldsymbol{u}_{1_n} - C_1\boldsymbol{u}_1\big] - \delta\boldsymbol{\lambda}_2^{\mathrm{T}}\big[B_2^{\mathrm{T}}\boldsymbol{u}_{2_n} - C_2\boldsymbol{u}_2\big]$$
$$+ \delta\boldsymbol{u}_1^{\mathrm{T}}\big[A_1^{\mathrm{T}}\boldsymbol{u}_{1_n} + C_1^{\mathrm{T}}\boldsymbol{\lambda}_1 - \boldsymbol{f}_1\big] + \delta\boldsymbol{u}_2^{\mathrm{T}}\big[A_2^{\mathrm{T}}\boldsymbol{u}_{2_n} + C_2^{\mathrm{T}}\boldsymbol{\lambda}_2 - \boldsymbol{f}_2\big] = 0, \tag{21}$$

where the various matrices in the above expression are given as:

$$A_\alpha = \frac{1}{\rho_\alpha}\int_{\partial\Omega_\alpha}\boldsymbol{\psi}_\alpha\boldsymbol{\phi}_\alpha^{\mathrm{T}}\,\mathrm{d}(\partial\Omega_\alpha), \tag{22a}$$

$$B_\alpha = \frac{1}{\rho_\alpha}\int_{\partial\Omega_\alpha}\boldsymbol{\psi}_\alpha\left[\frac{1}{2}\boldsymbol{\chi}_\alpha^{\mathrm{T}} + D_\alpha[\boldsymbol{\chi}_\alpha^{\mathrm{T}}]\right]\mathrm{d}(\partial\Omega_\alpha), \tag{22b}$$

$$C_\alpha = \frac{1}{\rho_\alpha}\int_{\partial\Omega_\alpha}\boldsymbol{\phi}_\alpha M_\alpha[\boldsymbol{\chi}_\alpha^{\mathrm{T}}]\,\mathrm{d}(\partial\Omega_\alpha), \tag{22c}$$

$$\boldsymbol{f}_\alpha = \frac{2}{\rho_\alpha}\int_{\Gamma_\alpha^{u_n}}h_\alpha\boldsymbol{\phi}_\alpha\,\mathrm{d}\Gamma_\alpha^{u_n}, \tag{22d}$$

with $\alpha = 1,2$. A detailed derivation and more explicit formulas for these expressions are given in the Appendix A.

Since, δu_{1_n}, δu_{2_n}, $\delta\lambda_1$, and $\delta\lambda_2$ are arbitrary within each of the subdomains Ω_1 and Ω_2, the terms they multiply in (21) must vanish. Thus:

$$u_{1_n} = B_1^{-T} C_1 u_1, \tag{23a}$$

$$u_{2_n} = B_2^{-T} C_2 u_2, \tag{23b}$$

$$\lambda_1 = B_1^{-1} A_1 u_1, \tag{24a}$$

$$\lambda_2 = B_2^{-1} A_2 u_2. \tag{24b}$$

Substituting Eqs. (23) and (24) into (21), yields:

$$\delta\hat{\mathscr{L}} = \delta u_1^T \left\{ \left[A_1^T B_1^{-T} C_1 + C_1^T B_1^{-1} A_1 \right] u_1 - f_1 \right\} + \delta u_2^T \left\{ \left[A_2^T B_2^{-T} C_2 + C_2^T B_2^{-1} A_2 \right] u_2 - f_2 \right\} = 0, \tag{25a}$$

or

$$\delta\hat{\mathscr{L}} = \delta u_1^T \left\{ K^{(1)} u_1 - f_1 \right\} + \delta u_2^T \left\{ K^{(2)} u_2 - f_2 \right\} = 0, \tag{25b}$$

where

$$K^{(\alpha)} = A_\alpha^T B_\alpha^{-T} C_\alpha + C_\alpha^T B_\alpha^{-1} A_\alpha, \quad \alpha = 1, 2. \tag{26}$$

3.2. Remarks

- Eq. (21), or equivalently (25), is the discrete form of the variational principle (13).
- As it can be seen from, e.g., Eqs. (16), u_α and λ_α are in $H^{\frac{1}{2}}(\partial\Omega_\alpha)$, whereas, u_{n_α} is in $H^{-\frac{1}{2}}(\partial\Omega_\alpha)$, with $\alpha = 1, 2$. It is thus justified to choose same-order polynomial approximations for ϕ_α and χ_α. We further opted to use same-order approximations for u_{n_α}, i.e., we let $\phi_\alpha \equiv \chi_\alpha \equiv \psi_\alpha$, $\alpha = 1, 2$. This choice of shape functions is permissible since the unknowns u_α, λ_α, and u_{n_α} in the integral equations are defined only on the boundaries and interfaces, and are completely independent of each other. Hence the LBB (Ladysenskaja–Babuška–Brezzi) condition that arises in mixed problems is immaterial in this problem. Examples of similar interface problems, involving exterior regions, can be found, e.g., in [2] and [5]. In these examples u and u_n were treated as independent variables, yet the existence, uniqueness, and convergence of the approximate solution has been proven without having to impose an LBB-type condition.
- The choice $\phi_\alpha = \chi_\alpha = \psi_\alpha$ leads to square matrices B_α. Provided B_α are non-singular, it is then possible to solve for u_{n_α} and λ_α in terms of the primary unknowns u_α separately within each subdomain, as shown in (23) and (24). This lends itself to the ready parallelization of the methodology.
- After applying this condensation procedure, the only remaining nodal unknowns are the pressures u_α, as seen in (25). The resulting matrices $K^{(\alpha)}$ are symmetric, since $K^{(\alpha)^T} = (A_\alpha^T B_\alpha^{-T} C_\alpha + C_\alpha^T B_\alpha^{-1} A_\alpha)^T = K^{(\alpha)}$.
- Eq. (26) (and similarly, (21) and (23)–(25)) involves inverses of B_α, which correspond to the (weighted) spatially discretized version of $\frac{1}{2}\lambda_\alpha + D[\lambda_\alpha]$ (see (15)). For potential problems (Laplace's operator), B_α are always non-singular, except for the trivial solution: as it can be readily seen from (15), when $\frac{1}{2}\lambda_\alpha + D[\lambda_\alpha] = 0$, then $u_\alpha = 0$ on the boundary, and since $\Delta u_\alpha = 0$ within the subdomain, then $u_\alpha = 0$ everywhere by a uniqueness argument. Similarly, by virtue of (18), $\lambda_\alpha = 0$ on the boundary.
  The situation, however, is different for the Helmholtz operator. Here $\frac{1}{2}\lambda_\alpha + D[\lambda_\alpha] = 0$ is singular if the frequency of excitation ω coincides with a natural frequency of the homogeneous Dirichlet problem defined over a subdomain Ω_α (such subdomain eigenfrequencies are not, in general, natural frequencies of the complete problem (1)). This means that the condensation approach represented by (23) fails for such frequencies, and consequently, that for these exceptional cases, in principle, one needs to solve the coupled equations for the complete set of variables u_α, λ_α, u_{n_α}, $\alpha = 1, 2$, all at once. However in [5,13] it was

ARTICLE IN PRESS

L.F. Kallivokas et al. / Comput. Methods Appl. Mech. Engrg. xxx (2004) xxx–xxx 11

found that when one uses variational methods for solving integral equations for exterior problems with breakdown frequencies, the errors become highly localized. It was observed that, in contrast to collocation methods, the condition number of the algebraic system remains small for all frequencies of excitation, ω, except when ω essentially coincides with an exceptional frequency. In fact, it was found that because of the highly localized nature of the singularity, a special effort was required to isolate the frequencies that would cause the resulting algebraic equations to become singular or ill-conditioned. Minute deviations from the breakdown frequencies led to well-conditioned systems and highly accurate solutions (see, e.g., Fig. 2 in [5], which also shows the unstable character of the collocation approach). This observation means that, in practice, the proposed condensation procedure will be applicable essentially at all frequencies. We conducted numerical experiments for our problem and found that for the breakdown frequencies of a subdomain to manifest in our numerical scheme, these eigenfrequencies must be prescribed to, at least, within five significant digits.

Naturally, the solution of the complete problem (1) is expected to break down for values of ω that coincide with a natural frequency of the original domain. As it was verified numerically, this is indeed the case.

- The variational principle based on (13) and (18) was derived here for interior problems, but is equally applicable to exterior multi-domain problems. All that is needed is to modify (11) to correspond to the exterior interface problem. Furthermore, the subdomain approach would automatically eliminate the artificial non-uniqueness associated with exterior problems that arises at eigenvalues of the interior problem. For example, as it was shown in e.g. [6] for exterior homogeneous domains, the difficulty is eliminated without need to resort to specialized schemes (e.g. Burton-Miller [14], Brakhage-Werner [15], Bielak et al. [5]).

3.3. Subdomain assembly—total algebraic system

To assemble the total algebraic system we now turn to the discrete form of the variational principle (25). Notice that δu_1^{T} and δu_2^{T} are arbitrary over $\widehat{\Gamma}_1 = \partial \Omega_1 \setminus \Gamma$ and $\widehat{\Gamma}_2 = \partial \Omega_2 \setminus \Gamma$, respectively; over Γ, δu_1^{T} and δu_2^{T} should be such that the continuity condition (4b) is satisfied. The latter calls for the partitioning of the unknown nodal pressure values; with the aid of Eqs. (26), the partitioning scheme will result in the following final algebraic system:

$$
\begin{bmatrix}
\boldsymbol{K}^{(1)}_{\hat{\Gamma}_1 \hat{\Gamma}_1} & \boldsymbol{K}^{(1)}_{\hat{\Gamma}_1 \Gamma} & 0 \\
\boldsymbol{K}^{(1)}_{\Gamma \hat{\Gamma}_1} & \boldsymbol{K}^{(1)}_{\Gamma \Gamma} + \boldsymbol{K}^{(2)}_{\Gamma \Gamma} & \boldsymbol{K}^{(2)}_{\Gamma \hat{\Gamma}_2} \\
0 & \boldsymbol{K}^{(2)}_{\hat{\Gamma}_2 \Gamma} & \boldsymbol{K}^{(2)}_{\hat{\Gamma}_2 \hat{\Gamma}_2}
\end{bmatrix}
\begin{bmatrix}
\boldsymbol{u}_{\hat{\Gamma}_1} \\
\boldsymbol{u}_\Gamma \\
\boldsymbol{u}_{\hat{\Gamma}_2}
\end{bmatrix}
=
\begin{bmatrix}
\boldsymbol{f}_{\hat{\Gamma}_1} \\
0 \\
\boldsymbol{f}_{\hat{\Gamma}_2}
\end{bmatrix},
\tag{27}
$$

where $\boldsymbol{u}_{\hat{\Gamma}_1}$ is the part of $\boldsymbol{u}_1$ on $\widehat{\Gamma}_1$, $\boldsymbol{u}_\Gamma$ consists of the unknowns on the interface Γ, and $\boldsymbol{u}_{\hat{\Gamma}_2}$ is the part of $\boldsymbol{u}_2$ on $\widehat{\Gamma}_2$; similarly for the force vector.

Once (27) is solved for the unknown nodal values of $\boldsymbol{u}$, the normal derivatives $\boldsymbol{u}_n$ and the Lagrange multipliers $\boldsymbol{\lambda}$ can be recovered using (23) and (24). Then, the solution within the subdomains Ω_1 and Ω_2 can be similarly recovered using the domain expressions (18); in terms of the approximate discrete values of λ_1 and λ_2:

$$
\mathfrak{u}_1(\boldsymbol{x}) = \mathfrak{D}_1[\lambda_1](\boldsymbol{x}) = \left[\int_{\partial \Omega_1} \boldsymbol{\chi}_1^{\mathrm{T}}(\boldsymbol{y}) \frac{\partial G(\boldsymbol{x}, \boldsymbol{y})}{\partial n_{\boldsymbol{y}}} d(\partial \Omega_1(\boldsymbol{y})) \right] \boldsymbol{\lambda_1}, \quad \boldsymbol{x} \in \Omega_1,
\tag{28a}
$$

$$\mathfrak{u}_2(\boldsymbol{x}) = \mathfrak{D}_2[\lambda_2](\boldsymbol{x}) = \left[\int_{\partial\Omega_2} \boldsymbol{\chi}_2^{\mathrm{T}}(\boldsymbol{y}) \frac{\partial G(\boldsymbol{x},\boldsymbol{y})}{\partial n_{\boldsymbol{y}}} \, \mathrm{d}(\partial\Omega_2(\boldsymbol{y})) \right] \boldsymbol{\lambda_2}, \quad \boldsymbol{x} \in \Omega_2. \tag{28b}$$

Alternatively, $\mathfrak{u}_1$ may be obtained from (6), and $\mathfrak{u}_2$ from a similar expression, in terms of their boundary values u_1, u_{1_n} on $\partial\Omega_1$, and u_2, u_{2_n} on $\partial\Omega_2$, respectively.

4. Numerical results

To assess the accuracy of the developed variational framework, we now consider several examples. These problems pertain to both the thermal and acoustic cases, involving the Laplace and Helmholtz operators, respectively. Problems involving Dirichlet data, Neumann data, or mixed boundary conditions were solved. We use piecewise quadratic approximations for the three variables u, u_n, and λ, in all our examples. We discuss the accuracy of the primary variable (temperature or pressure) on the subdomain boundaries (including the material interfaces), of the normal derivatives (heat fluxes and fluid accelerations) on the various boundary segments, and of the primary variables at points interior to the domains. For problems for which an exact solution is available, the accuracy is measured against the exact solution; for other problems we provide comparisons with results obtained using commercial finite element codes.

For thermal problems, we remark that the strong problem statement (1) need be modified in the following manner: (a) the governing Helmholtz operators in (1a) and (1b) are replaced by the Laplacian operators, and (b) the interface condition (1d) should read:

$$\kappa_1 u_{1_n}(\boldsymbol{x}) = \kappa_2 u_{2_n}(\boldsymbol{x}), \quad \boldsymbol{x} \in \Gamma, \tag{29}$$

where κ_1 and κ_2 are the thermal conductivities of Ω_1 and Ω_2, respectively. We further remark that, in the thermal case, only the non-frequency-dependent part of Maue's identity (second-term in (19)) will be exercised. In addition, the Green's function (8) need also be replaced by $\frac{1}{2\pi} \ln(z)$.

4.1. Thermal—concentric-circles case

We consider first the following BVP with pure Dirichlet boundary conditions, defined for the geometry shown in Fig. 2:
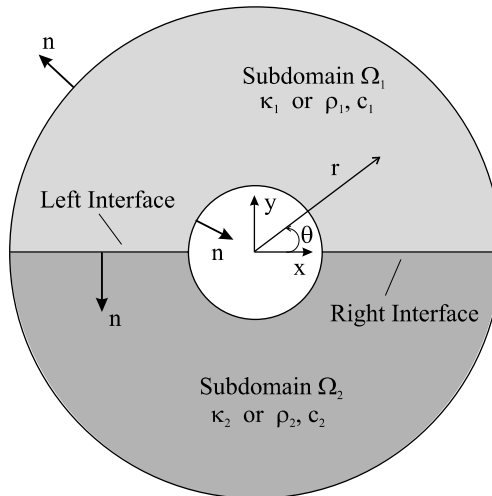

Fig. 2. Geometry of prototype problem—concentric-circles case (inner radius, $b = 0.25$, outer radius, $a = 1$).

ARTICLE IN PRESS

L.F. Kallivokas et al. / Comput. Methods Appl. Mech. Engrg. xxx (2004) xxx–xxx   13

$$u(r, \theta) = 100 \cos \theta, \quad \text{at } r = a,$$
$$u(r, \theta) = 50 \cos \theta, \quad \text{at } r = b, \tag{30a}$$
$$\kappa_1 = \kappa_2 = 1,$$

for which the exact solution for both the primary variable and its normal derivative are:

$$u(r, \theta) = \frac{1}{3} \left(280r + \frac{20}{r} \right) \cos \theta, \quad \text{for } b \leqslant r \leqslant a, \ 0 \leqslant \theta < 2\pi,$$

$$u_n(r, \theta) = \frac{1}{3} \left(280 - \frac{20}{r^2} \right) \cos \theta, \quad \text{at } r = a, \ 0 \leqslant \theta < 2\pi,$$

$$u_n(r, \theta) = -\frac{1}{3} \left(280 - \frac{20}{r^2} \right) \cos \theta, \quad \text{at } r = b, \ 0 \leqslant \theta < 2\pi, \tag{30b}$$

$$u_n(r, \theta) = \frac{1}{3} \left(280r + \frac{20}{r} \right) \sin \theta \frac{x}{r^2}, \quad \text{on the interface.}$$

We remark that in (30a) we used the same conductivity values for both subdomains: in such cases, our approach amounts to a domain decomposition method.

We used 56 elements (quadratic) for each subdomain (as per Fig. 3), with 32, 8, 8, and 8 elements on the outer circle, the left interface, the inner circle, and the right interface, respectively. Since (30a) imposes
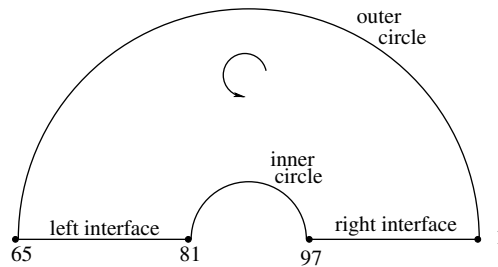

Fig. 3. Boundary discretization—subdomain Ω_1.

Table 1
Temperature (u) distribution on the left interface (Fig. 2) for problem (30)

x	SGBEM	Exact	Relative error (%)
−0.953	−95.843	−95.953	−0.115
−0.906	−91.909	−91.940	−0.033
−0.859	−87.945	−87.966	−0.024
−0.813	−84.016	−84.038	−0.027
−0.766	−80.152	−80.166	−0.017
−0.719	−76.345	−76.359	−0.018
−0.672	−72.620	−72.631	−0.014
−0.625	−68.991	−69.000	−0.013
−0.578	−65.482	−65.490	−0.013
−0.531	−62.127	−62.132	−0.008
−0.484	−58.965	−58.972	−0.012
−0.438	−56.071	−56.071	0.000
−0.391	−53.517	−53.525	−0.015
−0.344	−51.487	−51.477	0.020
−0.297	−50.153	−50.164	−0.024

ARTICLE IN PRESS

14   *L.F. Kallivokas et al. / Comput. Methods Appl. Mech. Engrg. xxx (2004) xxx–xxx*
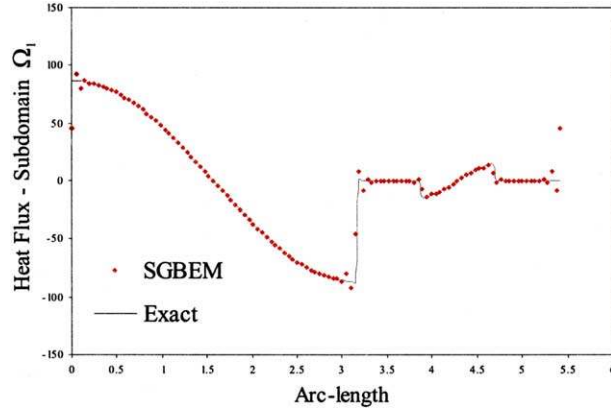
Fig. 4. Heat flux ($\kappa_1 u_n$) distribution along the perimeter of subdomain Ω_1 (Fig. 2) for problem (30).

Dirichlet data on both circles, the only unknowns for the condensed system (31) are the interface values of the primary variable. Table 1 below summarizes their values, and the relative error against the exact solution (30b), for the left interface (the right-interface values differ only in sign). As it can be readily seen from Table 1 the agreement between the exact and approximate solutions is excellent. By contrast, the normal derivatives suffer from loss of accuracy at the corner points: Fig. 4 depicts the distribution of the heat fluxes along the perimeter of subdomain Ω_1; in Fig. 4 the arc-length parameter denotes the cumulative length while traversing the boundary of Ω_1 in a counter-clockwise direction starting from the first node located in the rightmost end of Ω_1 (node 1 in Fig. 3). Notice that the interface fluxes are zero, as per (30b) for $y = 0$.

We observe that there is an abrupt oscillatory departure of the approximate solution (SGBEM) for the heat fluxes from the exact one, close to the corner points. In fact, the behavior, as it will be more clearly shown later, very closely resembles a Gibbs-type phenomenon. The difficulty is due to the fact that in formulating the problem, we have assumed smooth boundaries, for which the normal vector is uniquely defined at every boundary point. Clearly, in cases where corners are present, the normal vector is not uniquely defined, but rather multi-valued. Up to now, our formulation violates the non-uniqueness of the normals and merits intervention. A modified approach is discussed in Section 5. We further remark that the quality of the results for the primary variable remains unaffected despite the poor performance of the normal derivatives. Notice that the primary variables are obtained from the solution of the algebraic system (25) or (31); the normal derivatives and the Lagrange multipliers on the boundary are subsequently obtained by the matrix–vector products (23) and (24), respectively. Though the algebraic operators used in Eqs. (23) also appear in the algebraic system Eqs. (25) for the primary variable, notice that in Eqs. (25) they are preconditioned by the A_1^{T} or A_2^{T} subdomain matrices. We conjecture that the good quality of the solution for the primary variables despite the poor performance of the normal derivatives is due to the preconditioning operation described above.

To further illustrate the difficulties with the normal derivatives, we show, by example, that local refinement is not capable of restoring the quality of the solution near the corners. To this end, we experiment with the following BVP, also defined by making use of the concentric-circles geometry of Fig. 2, that results from a slight variation of (30a). Let:

$$
\begin{aligned}
u(r, \theta) &= 100 \sin \theta, \quad \text{at } r = a, \\
u(r, \theta) &= 0, \quad \text{at } r = b, \\
\kappa_1 &= \kappa_2 = 1,
\end{aligned}
$$

(31a)

ARTICLE IN PRESS

L.F. Kallivokas et al. / Comput. Methods Appl. Mech. Engrg. xxx (2004) xxx–xxx   15

for which the exact solution for both the primary variable and its normal derivative are:

$$u(r, \theta) = \frac{1}{3}\left(320r - \frac{20}{r}\right)\sin\theta, \quad \text{for } b \leqslant r \leqslant a, \ 0 \leqslant \theta < 2\pi,$$

$$u_n(r, \theta) = \frac{1}{3}\left(320 + \frac{20}{r^2}\right)\sin\theta, \quad \text{at } r = a, \ 0 \leqslant \theta < 2\pi,$$

$$u_n(r, \theta) = -\frac{1}{3}\left(320 + \frac{20}{r^2}\right)\sin\theta, \quad \text{at } r = b, \ 0 \leqslant \theta < 2\pi, \tag{31b}$$

$$u_n(r, \theta) = -\frac{1}{3}\left(320r - \frac{20}{r}\right)\cos\theta\,\frac{x}{r^2}, \quad \text{on the interface.}$$

Listed in Table 2 are the temperature values at the left interface for the above problem (31a). As expected, by (31b), the temperature should vanish at the interface, and indeed, the agreement is excellent. Fig. 5, by contrast, depicts the variation of the heat flux on the various segments of Ω_1 for discretizations of $\partial\Omega_1$ ranging from 14 to 448 elements. As it can be clearly seen, for coarse discretizations (e.g. 28 elements), the oscillatory behavior extends well beyond the corner points, whereas fine meshing (e.g. 448 elements) confines the departure from the exact solution to a narrow region close to the corner, where, however, again oscillations are present. In all cases, the value to which the solution converges at the corner is wrong: for example, at the intersection of the left interface with the outer circle, the exact values of the heat flux to the left and to the right of the intersection point should be 0 and −100, respectively, whereas the approximate converged value is −49.1.

Notice further that in the case of the inner circle (Fig. 5), the heat flux distribution is in excellent agreement with the exact: this is due to the fact that at the intersection points of the inner circle with the horizontal interfacial segments the normal derivative is zero from both sides of the intersection point, and therefore, the single-normal representation employed in the formulation is sufficient, in this case, for capturing the correct value.

4.2. Thermal—eccentric-circles case

We consider next a bimaterial interface problem to illustrate the applicability to general interface problems. Referring to the geometry depicted in Fig. 6, let (the problem geometry was borrowed from a similar problem presented in [9]):

Table 2
Temperature (u) distribution on the left interface (Fig. 2) for problem (31a)

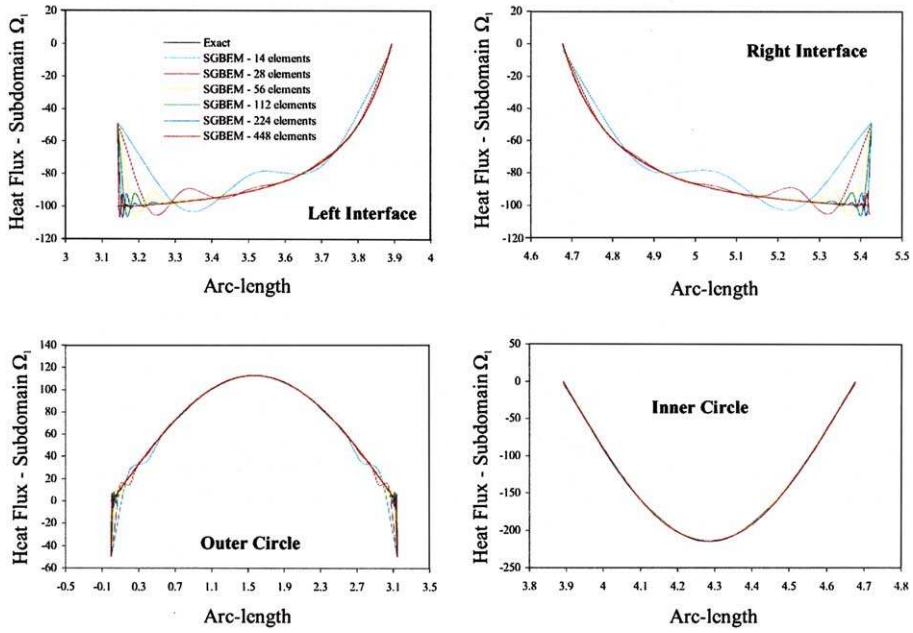| x	SGBEM	Exact
0.297	4.87E−15	0
0.344	1.47E−14	0
0.391	−8.59E−15	0
0.438	−7.00E−15	0
0.484	−2.77E−14	0
0.531	−2.38E−14	0
0.578	−2.01E−14	0
0.625	−2.70E−14	0
0.672	−2.56E−14	0
0.719	−1.01E−14	0
0.766	−2.05E−15	0
0.813	6.35E−15	0
0.859	−6.50E−15	0
0.906	−8.18E−15	0
0.953	−9.87E−15	0

Fig. 5. Heat flux ($\kappa_1 u_n$) distribution along the perimeter of subdomain Ω_1 (Fig. 2) for problem (31); element refinement.
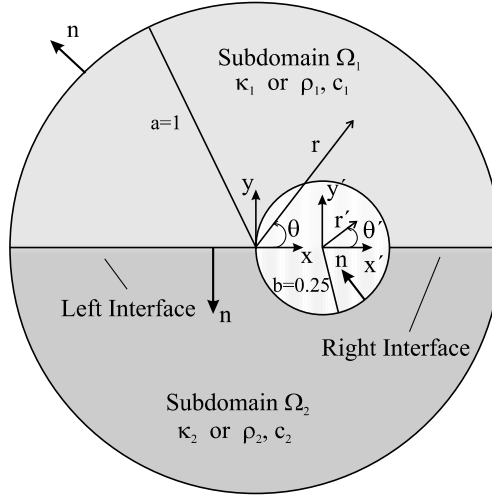

Fig. 6. Geometry of prototype problem—eccentric-circles case.

$$
\begin{aligned}
u(r) &= 100, \quad \text{at } r = a, \ \theta = 0 \ldots \pi, \\
u(r') &= 0, \quad \text{at } r' = b, \ \theta' = 0 \ldots \pi, \\
u_r(r) &= 0, \quad \text{at } r = a, \ \theta = \pi \ldots 2\pi, \\
u_r(r') &= 0, \quad \text{at } r' = b, \ \theta' = \pi \ldots 2\pi, \\
\kappa_1 &= 1, \quad \text{and} \quad \kappa_2 = 0.5.
\end{aligned}
\tag{32}
$$
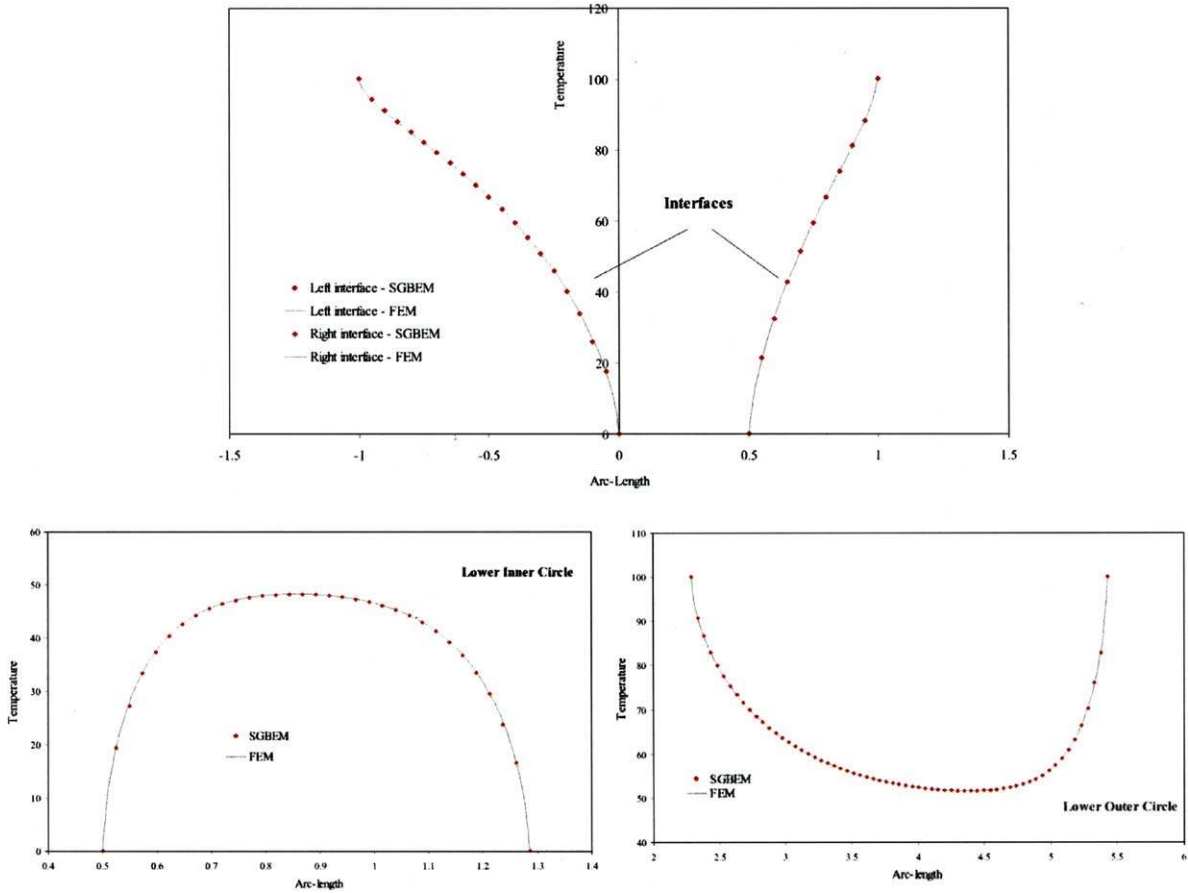
Fig. 7. Temperature (*u*) distribution on the interface and the lower inner and outer circles (Fig. 6) for problem (32).

Fig. 7 shows a comparison between the SGBEM solution and a finite element solution obtained using a commercial code (ANSYS; no exact solution is available for this problem) for the temperature distribution along the bimaterial interface and along the insulated (zero flux) lower inner and outer semi-circles, respectively. The agreement between the two solutions is again excellent. By contrast, Fig. 8 shows the heat fluxes along the perimeter of both subdomains, including the segments for which the flux was prescribed. Whereas away from the corners, the finite element and SGBEM solutions are graphically indistinguishable, near the corners the oscillatory behavior of the normals, identified earlier for the homogeneous cases, is present here as well.

4.3. Acoustic—concentric- and eccentric-circles cases

In order to show the applicability of the approach to the acoustic case we again distinguish two cases corresponding to the two geometries of concentric and eccentric circles, Figs. 2 and 6, respectively. There are only minor differences between the thermal and acoustic cases: (a) the Green's function (8), (b) the complex nature of the solution for the primary variable (pressure) and its normal derivative (fluid acceleration), and (c) the frequency-dependent part of Maue's identity (19). We start with the analog to problem (30a), i.e., let:
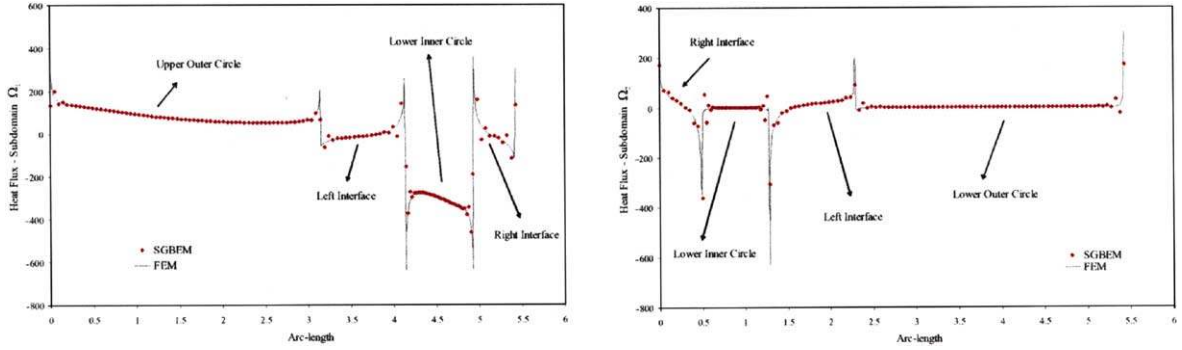
Fig. 8. Heat flux distribution along the perimeter of both subdomains Ω_1 and Ω_2 for problem (32).

$$u(r,\theta) = (100 + i100)\cos\theta, \quad \text{at } r = a,$$
$$u(r,\theta) = (50 + i50)\cos\theta, \quad \text{at } r = b, \tag{33a}$$
$$\rho_1 = \rho_2 = 1, \quad c_1 = c_2 = 1, \quad \text{and} \quad \omega = 1,$$

for which the exact solution for both the primary variable and its normal derivative are:

$$u(r,\theta) = [\beta_1 H_0^{(1)}(kr) + \beta_2 H_0^{(2)}(kr)]\cos\theta, \quad \text{for } b \leqslant r \leqslant a, \ 0 \leqslant \theta < 2\pi,$$

with

$$\beta_1 = \frac{(100 + i100)H_0^{(2)}(kb) - (50 + i50)H_0^{(2)}(ka)}{H_0^{(1)}(ka)H_0^{(2)}(kb) - H_0^{(2)}(ka)H_0^{(1)}(kb)},$$

$$\beta_2 = \frac{(50 + i50)H_0^{(1)}(ka) - (100 + i100)H_0^{(1)}(kb)}{H_0^{(1)}(ka)H_0^{(2)}(kb) - H_0^{(2)}(ka)H_0^{(1)}(kb)}, \tag{33b}$$

$$u_n(r,\theta) = -k[\beta_1 H_1^{(1)}(kr) + \beta_2 H_1^{(2)}(kr)]\cos\theta, \quad \text{at } r = a, \ 0 \leqslant \theta < 2\pi,$$
$$u_n(r,\theta) = k[\beta_1 H_1^{(1)}(kr) + \beta_2 H_1^{(2)}(kr)]\cos\theta, \quad \text{at } r = b, \ 0 \leqslant \theta < 2\pi,$$
$$u_n(r,\theta) = [\beta_1 H_0^{(1)}(kr) + \beta_2 H_0^{(2)}(kr)]\sin\theta \frac{x}{r^2}, \quad \text{on the interface.}$$

We are considering here a single value of the frequency of excitation, for which all the necessary matrices are non-singular. Listed in Table 3 is the real part of the complex-valued pressure along the left interface; again, the agreement between exact and the SGBEM solution is excellent. The distribution of the real part of the fluid acceleration along the boundary $\partial\Omega_1$ is depicted in Fig. 9. The same trends identified earlier for the thermal case are observed here as well.

As a last problem for the Helmholtz operator, we considered the counterpart to the eccentric case (32). The BVP was defined as:

$$u(r) = (100 + i100), \quad \text{at } r = a, \ \theta = 0 \ldots \pi,$$
$$u(r') = 0, \quad \text{at } r' = b, \ \theta' = 0 \ldots \pi,$$
$$u_r(r) = 0, \quad \text{at } r = a, \ \theta = \pi \ldots 2\pi, \tag{34}$$
$$u_r(r') = 0, \quad \text{at } r' = b, \ \theta' = \pi \ldots 2\pi,$$
$$\rho_1 = 1, \quad \rho_2 = 2, \quad c_1 = c_2 = 1, \quad \text{and} \quad \omega = 1.$$

Table 3
Real part of the pressure (u) distribution on the left interface (Fig. 2) for problem (33)

| x	SGBEM	Exact	Relative error (%)
−0.969	−97.980	−98.059	−0.080
−0.938	−96.026	−96.060	−0.035
−0.906	−93.989	−94.007	−0.018
−0.875	−91.882	−91.902	−0.022
−0.844	−89.737	−89.748	−0.013
−0.813	−87.538	−87.549	−0.013
−0.781	−85.301	−85.309	−0.010
−0.750	−83.024	−83.032	−0.009
−0.719	−80.716	−80.722	−0.008
−0.688	−78.380	−78.385	−0.007
−0.656	−76.023	−76.027	−0.006
−0.625	−73.651	−73.655	−0.005
−0.594	−71.272	−71.275	−0.004
−0.563	−68.897	−68.899	−0.003
−0.531	−66.534	−66.536	−0.003
−0.500	−64.200	−64.201	−0.001
−0.469	−61.908	−61.909	−0.001
−0.438	−59.683	−59.681	0.003
−0.406	−57.545	−57.544	0.001
−0.375	−55.539	−55.533	0.011
−0.344	−53.695	−53.693	0.004
−0.313	−52.102	−52.088	0.026
−0.281	−50.829	−50.812	0.034
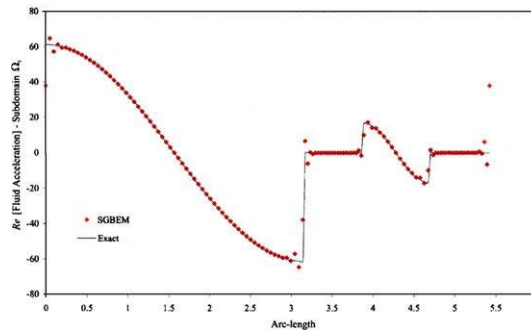
Fig. 9. Real part of fluid acceleration along the perimeter of subdomain Ω_1 (Fig. 2) for problem (33).

Fig. 10 compares the real part of the pressure along the bimaterial interface as obtained using the SGBEM approach presented herein against a finite element solution. The agreement between the two solutions is again quite satisfactory.

4.4. Subdomain interior solutions

Numerical solutions for the primary variables are attainable in the interior at the post-processing phase. First the algebraic system (25) is solved to obtain the primary variable on the boundaries (non-Dirichlet parts of external boundaries and on the material interfaces). Then, using (24a) and
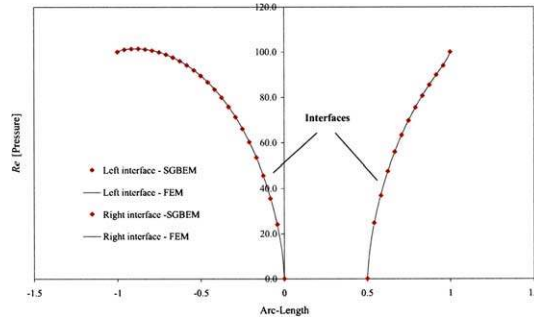
Fig. 10. Real part of pressure (u) on the interface (Fig. 6) for problem (34).

(24b), the Lagrange multipliers are recovered via matrix–vector products on the subdomain boundaries. Solutions interior to the subdomains are then readily calculated via the double-layer domain operators (18a) and (18b), or their discrete counterparts (32a) and (32b), respectively. Fig. 11 depicts the temperature distribution over the entire domain for the bimaterial interface problem (32). The SGBEM solution was obtained with 110 quadratic boundary elements. In order for the FEM solution to attain an accuracy comparable to that of the SGBEM, we used 41,469 bilinear elements resulting in 41,981 degrees of freedom. The SGBEM requires, of course, that the integrals in (28a) and (28b) be evaluated at the points of interest within the domain. Using the SGBEM solution we obtained the temperature at all interior points of the finite element mesh in order to construct contours with the same mesh density. We also compared the two solutions on a point-per-point basis (with respect to the FEM solution) (Fig. 11c): the agreement throughout the domain is excellent (the highest recorded difference was less than 1%).
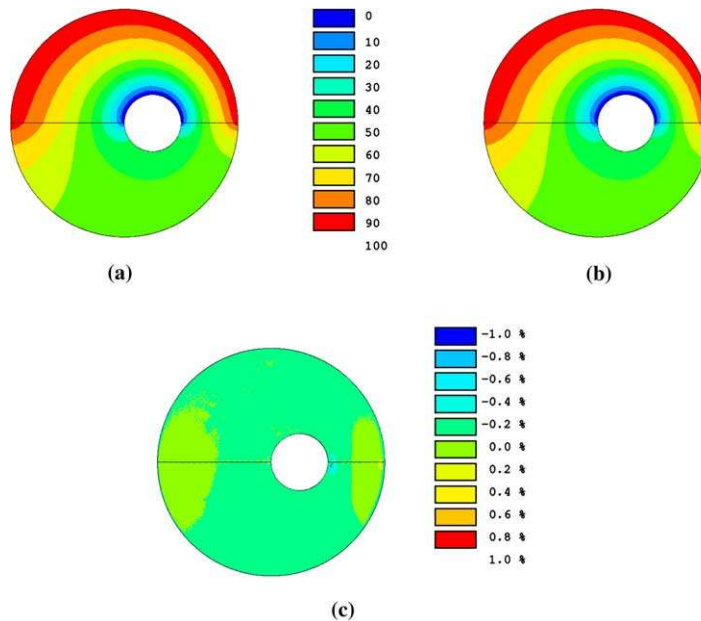

Fig. 11. Temperature distribution for the bimaterial interface problem (32): (a) FEM; (b) SGBEM; (c) pointwise difference in percent.
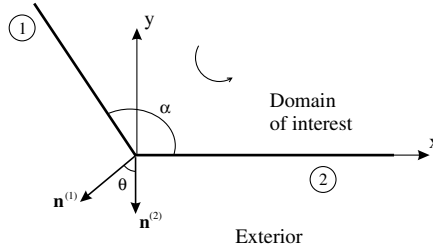
Fig. 12. Corner geometry.

5. Variational corner treatment

As discussed before, the numerical results described thus far show excellent agreement in the primary variable; however, the solution for the normal derivatives deteriorates when a sharp corner is approached. In fact, it appears that the deterioration is not localized to the corner: the corner errors migrate to neighboring elements as well. Away from the corner the solution for the normal derivatives improves significantly to attain, given enough elements, a quality similar to the one attained by the primary variable. [2] Refinement, whether local (comprising only elements neighboring the corner) or global, does not seem to alleviate the problem.

As discussed earlier, the difficulty with the normal derivatives originates from our implementation: we have used a single-node numerical implementation to represent subdomain corners. This implies a single unknown for the normal derivative at a corner; however, the normal vector is not single-valued, but multi-valued, for there exists an infinity of directions along which one can define the normal at a corner. Even in the limiting case where only two normal directions are considered associated with the two elements connecting to a corner (Fig. 12), our implementation accounts for only one (average) direction.

We remark that in our implementation all elements terminate at a corner; that is, there is no element spanning a corner since the mathematical development, as presented, accounts only for smooth boundary curves. We further remark that even if an element were used to span the corner in a manner that accounts for the sharp geometric discontinuity (unlikely to be encountered in numerical implementations), and one were to include the proper corner term in the jump conditions instead of the $\frac{1}{2}$ term, such an approach will not be capable of alleviating the problem we encounter here, for it would still not account for the multi-valued normals at the corners. Thus, in this section, we modify our variational framework to account for the solution at the corners, while still operating on piecewise smooth boundary curves.

Our approach for remedying the difficulty with the normal derivatives originates from the projection theorem in elasticity [16]. The approach is not new and can be found in the early boundary element literature (e.g. [17]). The central idea is that the normal derivatives to the left and to the right of a corner are not independent of each other: as it will be shown below, they are connected with the one-sided tangential derivative, and thus, in turn, with the Dirichlet data on the boundary. To fix ideas, let us consider first the geometry shown in Fig. 12, where the straight segments identified with encircled numbers 1 and 2 represent the tangents to the (generally) curved elements that meet at a sharp corner. The tangents form an interior angle of α ($\theta = \pi - \alpha$). Shown in the figure are also the two outward unit normals to segments 1 and 2. We have aligned a local coordinate system with segment 2; in this system, and for any continuous field u, there holds:

$$\frac{\partial u}{\partial n^{(1)}} = \frac{\partial u}{\partial x} n_x^{(1)} + \frac{\partial u}{\partial y} n_y^{(1)}, \tag{35a}$$

---

[2] Given the extremely small relative errors we opted not to study errors in appropriate norms.

$$\frac{\partial u}{\partial n^{(2)}} = \frac{\partial u}{\partial x} n_x^{(2)} + \frac{\partial u}{\partial y} n_y^{(2)}, \tag{35b}$$

where $n_x^{(1)}$ and $n_y^{(1)}$ represent the directional cosines (or components) of the unit normal vector $\boldsymbol{n}^{(1)}$; similarly for $n_x^{(2)}$ and $n_y^{(2)}$. These components in the local system are:

$$n_x^{(1)} = -\sin\theta = -\sin\alpha, \quad n_y^{(1)} = -\cos\theta = \cos\alpha, \tag{36a}$$

$$n_x^{(2)} = 0, \quad n_y^{(2)} = -1. \tag{36b}$$

Substituting (36) into (35a), while recognizing that $\frac{\partial u}{\partial y} \equiv -\frac{\partial u}{\partial n^{(2)}}$ and $\frac{\partial u}{\partial x} \equiv \frac{\partial u}{\partial s^{(2)}}$, where $s^{(2)}$ denotes arc-length along segment 2, yields:

$$\frac{\partial u}{\partial n^{(1)}} = -\cos\alpha \frac{\partial u}{\partial n^{(2)}} - \sin\alpha \frac{\partial u}{\partial s^{(2)}}. \tag{37}$$

Clearly, (37) suggests that the two normals are not independent; our remedy relies on (37). Specifically, first we allow for two values for the normal derivative per corner. This, in turn, implies the presence of a double node (one node from each side of the corner with identical coordinates) (Fig. 13).

We describe the necessary modifications to the discrete form of the variational principle (25). To fix ideas, we consider a single domain Ω (Fig. 14) with a single corner at C, modeled using a double-node representation.

The boundary of Ω is discretized using $N + 1$ nodes (included in the $N + 1$ nodes is the double corner node at C (Fig. 14)). Accordingly, there are N primary variable unknowns ($\boldsymbol{u}$), N Lagrange multipliers
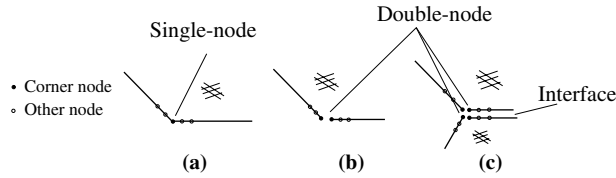

Fig. 13. (a) Single-node geometry (single subdomain); (b) double-node geometry (single subdomain); (c) double double-node geometry (two subdomains).
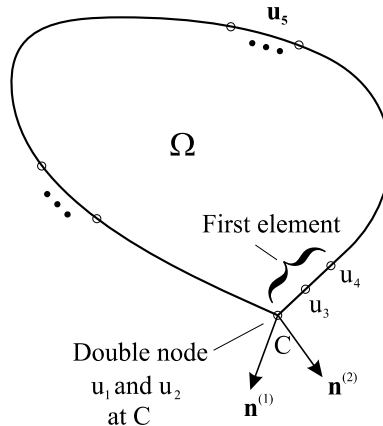

Fig. 14. Partitioning of single-corner boundary $\partial\Omega$.

(λ), and $N + 1$ normal derivatives (u_n). We partition the unknown nodal vectors as follows: let u_1, u_2 denote the unknown nodal primary variables of the double node (both scalar quantities); let u_3, u_4 denote the remaining nodal values of the primary variable on the first element to the right of the C (also scalars) (Fig. 14); let u_5 denote the rest of the nodal primary unknowns over $\partial\Omega$; u_5 has a dimension of $(N - 3) \times 1$. We partition the normal derivatives and the Lagrange multipliers in a similar manner. We compute the subdomain matrices using the procedure and expressions given in Section 3, with the proviso that no element spans the double node. Next, we rewrite the discrete form (25) to reflect the introduction of the partitioning:

$$
\delta\hat{\mathscr{L}} = \left[\delta u_n^{(1)}\ \delta u_n^{(2)}\ \delta u_n^{(3)}\ \delta u_n^{(4)}\ \boldsymbol{\delta u_n^{(5)}}^{\mathrm{T}}\right]\left\{\begin{bmatrix} A_{11} & A_{12} & A_{13} & A_{14} & \boldsymbol{A_{15}} \\ A_{21} & A_{22} & A_{23} & A_{24} & \boldsymbol{A_{25}} \\ A_{31} & A_{32} & A_{33} & A_{34} & \boldsymbol{A_{35}} \\ A_{41} & A_{42} & A_{43} & A_{44} & \boldsymbol{A_{45}} \\ \boldsymbol{A_{51}} & \boldsymbol{A_{52}} & \boldsymbol{A_{53}} & \boldsymbol{A_{54}} & \boldsymbol{A_{55}} \end{bmatrix}\begin{bmatrix} u_1 \\ u_2 \\ u_3 \\ u_4 \\ \boldsymbol{u_5} \end{bmatrix}\right.
$$

$$
\times \begin{bmatrix} B_{11} & B_{12} & B_{13} & B_{14} & \boldsymbol{B_{15}} \\ B_{21} & B_{22} & B_{23} & B_{24} & \boldsymbol{B_{25}} \\ B_{31} & B_{32} & B_{33} & B_{34} & \boldsymbol{B_{35}} \\ B_{41} & B_{42} & B_{43} & B_{44} & \boldsymbol{B_{45}} \\ \boldsymbol{B_{51}} & \boldsymbol{B_{52}} & \boldsymbol{B_{53}} & \boldsymbol{B_{54}} & \boldsymbol{B_{55}} \end{bmatrix}\begin{bmatrix} \lambda_1 \\ \lambda_2 \\ \lambda_3 \\ \lambda_4 \\ \lambda_5 \end{bmatrix}\right\} - \left[\delta\lambda_1\ \delta\lambda_2\ \delta\lambda_3\ \delta\lambda_4\ \boldsymbol{\delta\lambda_5}^{\mathrm{T}}\right]
$$

$$
\times \left\{\begin{bmatrix} B_{11}^{\mathrm{T}} & B_{12}^{\mathrm{T}} & B_{13}^{\mathrm{T}} & B_{14}^{\mathrm{T}} & \boldsymbol{B_{15}^{\mathrm{T}}} \\ B_{21}^{\mathrm{T}} & B_{22}^{\mathrm{T}} & B_{23}^{\mathrm{T}} & B_{24}^{\mathrm{T}} & \boldsymbol{B_{25}^{\mathrm{T}}} \\ B_{31}^{\mathrm{T}} & B_{32}^{\mathrm{T}} & B_{33}^{\mathrm{T}} & B_{34}^{\mathrm{T}} & \boldsymbol{B_{35}^{\mathrm{T}}} \\ B_{41}^{\mathrm{T}} & B_{42}^{\mathrm{T}} & B_{43}^{\mathrm{T}} & B_{44}^{\mathrm{T}} & \boldsymbol{B_{45}^{\mathrm{T}}} \\ \boldsymbol{B_{51}^{\mathrm{T}}} & \boldsymbol{B_{52}^{\mathrm{T}}} & \boldsymbol{B_{53}^{\mathrm{T}}} & \boldsymbol{B_{54}^{\mathrm{T}}} & \boldsymbol{B_{55}^{\mathrm{T}}} \end{bmatrix}\begin{bmatrix} u_n^{(1)} \\ u_n^{(2)} \\ u_n^{(3)} \\ u_n^{(4)} \\ \boldsymbol{u_n^{(5)}} \end{bmatrix} - \begin{bmatrix} C_{11} & C_{12} & C_{13} & C_{14} & \boldsymbol{C_{15}} \\ C_{21} & C_{22} & C_{23} & C_{24} & \boldsymbol{C_{25}} \\ C_{31} & C_{32} & C_{33} & C_{34} & \boldsymbol{C_{35}} \\ C_{41} & C_{42} & C_{43} & C_{44} & \boldsymbol{C_{45}} \\ \boldsymbol{C_{51}} & \boldsymbol{C_{52}} & \boldsymbol{C_{53}} & \boldsymbol{C_{54}} & C_{55} \end{bmatrix}\begin{bmatrix} u_1 \\ u_2 \\ u_3 \\ u_4 \\ \boldsymbol{u_5} \end{bmatrix}\right\}
$$

$$
+ \left[\delta u_1\ \delta u_2\ \delta u_3\ \delta u_4\ \boldsymbol{\delta u_5}^{\mathrm{T}}\right]\left\{\begin{bmatrix} A_{11}^{\mathrm{T}} & A_{12}^{\mathrm{T}} & A_{13}^{\mathrm{T}} & A_{14}^{\mathrm{T}} & \boldsymbol{A_{15}^{\mathrm{T}}} \\ A_{21}^{\mathrm{T}} & A_{22}^{\mathrm{T}} & A_{23}^{\mathrm{T}} & A_{24}^{\mathrm{T}} & \boldsymbol{A_{25}^{\mathrm{T}}} \\ A_{31}^{\mathrm{T}} & A_{32}^{\mathrm{T}} & A_{33}^{\mathrm{T}} & A_{34}^{\mathrm{T}} & \boldsymbol{A_{35}^{\mathrm{T}}} \\ A_{41}^{\mathrm{T}} & A_{42}^{\mathrm{T}} & A_{43}^{\mathrm{T}} & A_{44}^{\mathrm{T}} & \boldsymbol{A_{45}^{\mathrm{T}}} \\ \boldsymbol{A_{51}^{\mathrm{T}}} & \boldsymbol{A_{52}^{\mathrm{T}}} & \boldsymbol{A_{53}^{\mathrm{T}}} & \boldsymbol{A_{54}^{\mathrm{T}}} & \boldsymbol{A_{55}^{\mathrm{T}}} \end{bmatrix}\begin{bmatrix} u_n^{(1)} \\ u_n^{(2)} \\ u_n^{(3)} \\ u_n^{(4)} \\ \boldsymbol{u_n^{(5)}} \end{bmatrix}\right.
$$

$$
\left. - \begin{bmatrix} C_{11}^{\mathrm{T}} & C_{12}^{\mathrm{T}} & C_{13}^{\mathrm{T}} & C_{14}^{\mathrm{T}} & \boldsymbol{C_{15}^{\mathrm{T}}} \\ C_{21}^{\mathrm{T}} & C_{22}^{\mathrm{T}} & C_{23}^{\mathrm{T}} & C_{24}^{\mathrm{T}} & \boldsymbol{C_{25}^{\mathrm{T}}} \\ C_{31}^{\mathrm{T}} & C_{32}^{\mathrm{T}} & C_{33}^{\mathrm{T}} & C_{34}^{\mathrm{T}} & \boldsymbol{C_{35}^{\mathrm{T}}} \\ C_{41}^{\mathrm{T}} & C_{42}^{\mathrm{T}} & C_{43}^{\mathrm{T}} & C_{44}^{\mathrm{T}} & \boldsymbol{C_{45}^{\mathrm{T}}} \\ \boldsymbol{C_{51}^{\mathrm{T}}} & \boldsymbol{C_{52}^{\mathrm{T}}} & \boldsymbol{C_{53}^{\mathrm{T}}} & \boldsymbol{C_{54}^{\mathrm{T}}} & \boldsymbol{C_{55}^{\mathrm{T}}} \end{bmatrix}\begin{bmatrix} \lambda_1 \\ \lambda_2 \\ \lambda_3 \\ \lambda_4 \\ \lambda_5 \end{bmatrix} - \begin{bmatrix} f_1 \\ f_2 \\ f_3 \\ f_4 \\ \boldsymbol{f_5} \end{bmatrix}\right\} = 0. \tag{38}
$$

Next, we use the constraint condition (37) to eliminate $u_n^{(1)}$ from (38). Accordingly:

$$
u_n^{(1)} = -u_n^{(2)}\cos\alpha - u_s^{(2)}\sin\alpha = -\gamma u_n^{(2)} - (\epsilon_2 u_2 + \epsilon_3 u_3 + \epsilon_4 u_4), \tag{39a}
$$

and similarly,

$$\delta u_n^{(1)} = -\gamma \delta u_n^{(2)} - (\epsilon_2 \delta u_2 + \epsilon_3 \delta u_3 + \epsilon_4 \delta u_4), \tag{39b}$$

where ϵ_2, ϵ_3, ϵ_4 are the coefficients of the finite difference approximation for the tangential derivative in the above relations (invoked only over the first element). For example, for a second-order forward scheme:

$$\epsilon_2 = -\frac{3}{s} \sin \alpha, \quad \epsilon_3 = -\frac{1}{s} \sin \alpha, \tag{40}$$

$$\epsilon_4 = \frac{4}{s} \sin \alpha, \quad \text{with } s = \text{element length}.$$

Furthermore, we explicitly impose equality on the primary variable and the Lagrange multiplier at the double node, i.e.:

$$u_1 = u_2, \quad \delta u_1 = \delta u_2, \quad \lambda_1 = \lambda_2, \quad \delta \lambda_1 = \delta \lambda_2. \tag{41}$$

The introduction of (39) and (40) in (38) yields the modified discrete form of the variational principle (written here for one domain only):

$$\delta \hat{\mathscr{L}} = \delta \hat{u}_n^{\mathrm{T}}[\hat{A}u - \hat{B}\lambda] - \delta \lambda^{\mathrm{T}}[\hat{B}^{\mathrm{T}}\hat{u}_n - \hat{C}u] + \delta u^{\mathrm{T}}[\hat{A}^{\mathrm{T}}\hat{u}_n + \hat{C}^{\mathrm{T}}\lambda - \hat{D}u - f] = 0, \tag{42}$$

where the modified matrices are now defined as:

$$\hat{A} = \begin{bmatrix} A_{21} + A_{22} - \gamma(A_{11} + A_{12}) & A_{23} - \gamma A_{13} & A_{24} - \gamma A_{14} & \mathbf{A_{25} - \gamma A_{15}} \\ A_{31} + A_{32} & A_{33} & A_{34} & \mathbf{A_{35}} \\ A_{41} + A_{42} & A_{43} & A_{44} & \mathbf{A_{45}} \\ \mathbf{A_{51} + A_{52}} & \mathbf{A_{53}} & \mathbf{A_{54}} & \mathbf{A_{55}} \end{bmatrix}, \tag{43a}$$

$$\hat{B} = \begin{bmatrix} B_{21} + B_{22} - \gamma(B_{11} + B_{12}) & B_{23} - \gamma B_{13} & B_{24} - \gamma B_{14} & \mathbf{B_{25} - \gamma B_{15}} \\ B_{31} + B_{32} & B_{33} & B_{34} & \mathbf{B_{35}} \\ B_{41} + B_{42} & B_{43} & B_{44} & \mathbf{B_{45}} \\ \mathbf{B_{51} + B_{52}} & \mathbf{B_{53}} & \mathbf{B_{54}} & \mathbf{B_{55}} \end{bmatrix}, \tag{43b}$$

$$\hat{C} = \begin{bmatrix} C_{11} + C_{12} + C_{21} + C_{22} + \epsilon_2(B_{11} + B_{12}) & C_{13} + C_{23} + \epsilon_3(B_{11} + B_{12}) & C_{14} + C_{24} + \epsilon_4(B_{11} + B_{12}) & \mathbf{C_{15} + C_{25}} \\ C_{31} + C_{32} + \epsilon_2 B_{13} & C_{33} + \epsilon_3 B_{13} & C_{34} + \epsilon_4 B_{13} & \mathbf{C_{35}} \\ C_{41} + C_{42} + \epsilon_2 B_{14} & C_{43} + \epsilon_3 B_{14} & C_{44} + \epsilon_4 B_{14} & \mathbf{C_{45}} \\ \mathbf{C_{51} + C_{52}} + \epsilon_2 \mathbf{B_{15}} & \mathbf{C_{53}} + \epsilon_3 \mathbf{B_{15}} & \mathbf{C_{54}} + \epsilon_4 \mathbf{B_{15}} & \mathbf{C_{55}} \end{bmatrix}, \tag{43c}$$

$$\hat{D} = \begin{bmatrix} 2\epsilon_2(A_{11} + A_{12}) & \epsilon_3(A_{11} + A_{12}) + \epsilon_2 A_{13} & \epsilon_4(A_{11} + A_{12}) + \epsilon_2 A_{14} & \epsilon_2 \mathbf{A_{15}} \\ \epsilon_3(A_{11} + A_{12}) + \epsilon_2 A_{13} & 2\epsilon_3 A_{13} & \epsilon_3 A_{14} + \epsilon_4 A_{13} & \epsilon_3 \mathbf{A_{15}} \\ \epsilon_4(A_{11} + A_{12}) + \epsilon_2 A_{14} & \epsilon_3 A_{14} + \epsilon_4 A_{13} & 2\epsilon_4 A_{14} & \epsilon_4 \mathbf{A_{15}} \\ \epsilon_2 \mathbf{A_{15}} & \epsilon_3 \mathbf{A_{15}} & \epsilon_4 \mathbf{A_{15}} & \mathbf{0} \end{bmatrix}, \tag{43d}$$

and the modified normal derivative nodal vector is given by:

$$\hat{u}_n^{\mathrm{T}} = [\, u_n^{(2)} \quad u_n^{(3)} \quad u_n^{(4)} \quad \mathbf{u_n^{(5)}}^{\mathrm{T}} \,]. \tag{44}$$

Using arguments similar to those used in the numerical implementation Section 3, the final modified discrete variational form capable of accommodating corners, can be written as (for one domain; similarly for multiple domains):

$$\delta\boldsymbol{u}^{\mathrm{T}}\{[\hat{A}^{\mathrm{T}}\hat{B}^{-\mathrm{T}}\hat{C} + \hat{C}^{\mathrm{T}}\hat{B}^{-1}\hat{A} - \hat{D}]\boldsymbol{u} - \boldsymbol{f}\} = 0. \tag{45}$$

Notice that the discrete form (45), derived here for two-dimensional problems, is *symmetric*. We remark that, in principle, the same variational treatment of corners may be followed in three-dimensional problems, albeit at a slight increase in complexity: for example, relations similar to (35) would now need to involve the normal and tangential derivatives corresponding to each of the three planes intersecting at a corner.

We applied the modified statement (45) to the concentric-circles Laplace problem (31) for which we had shown that refinement does not improve the behavior of the normal derivatives at corners (see Fig. 5). Fig. 15 shows three curves: the exact solution, the solution obtained with the original form (25) for 56 elements, and the solution obtained using the modified form (45) (same number of elements). The oscillatory behavior has now been eliminated with the result that the exact and modified solutions become indistinguishable.

As a last illustration of the modified discrete variational form (45), we consider a domain that includes both interface and non-interface corners. The geometry is depicted in Fig. 16 (150 quadratic isoparametric elements were used for the discretization of the various boundary segments). The associated BVP is defined as:

$$\kappa_1\Delta u_1 = 0, \quad \text{in } \Omega_1, \qquad \kappa_2\Delta u_2 = 0, \quad \text{in } \Omega_2, \tag{46a}$$

$$u_1(0,y) = 0, \quad \text{and} \quad u_1(L,y) = 0, \ 0 \leqslant y \leqslant \frac{h}{2},$$
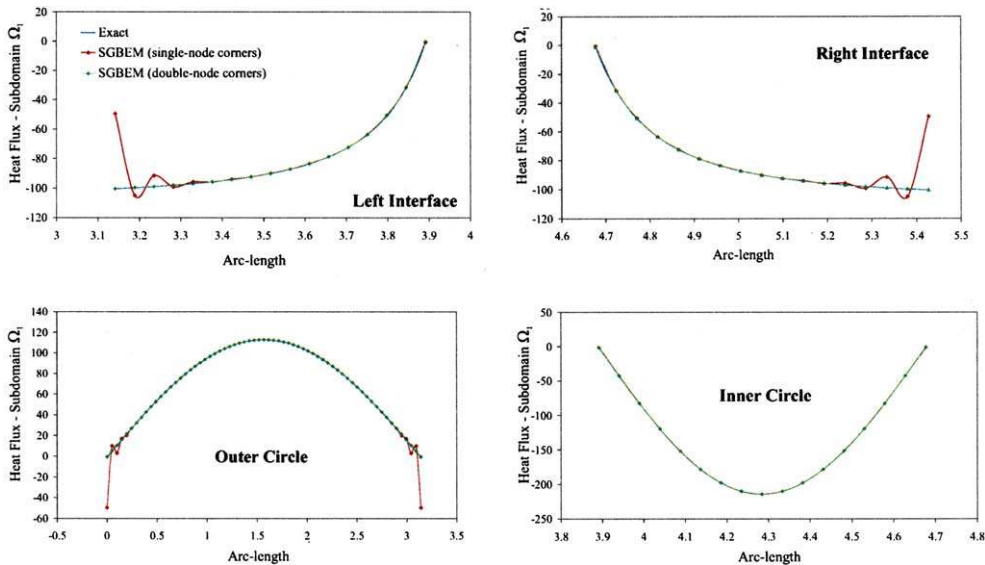

Fig. 15. Heat flux ($\kappa_1 u_n$) distribution along the perimeter of subdomain Ω_1 (Fig. 2) for problem (31) using the modified variational statement (45).
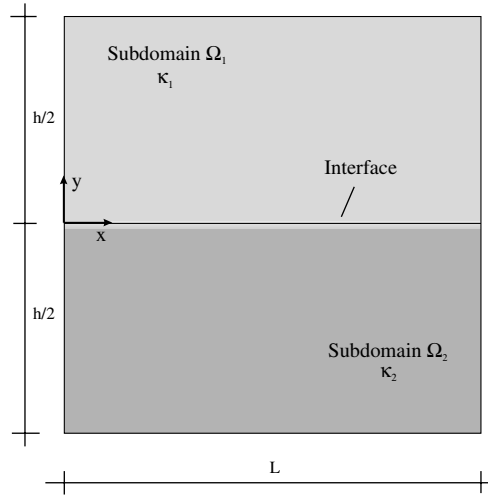
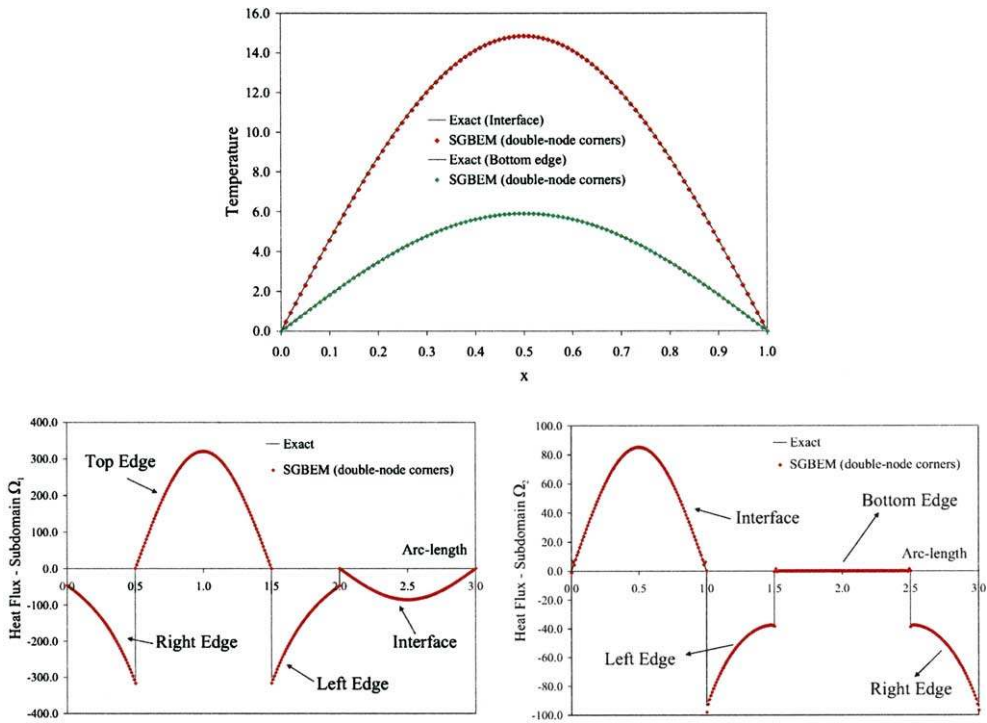Fig. 16. Geometry of rectangular prototype problem.

Fig. 17. Distribution of temperatures on the interface and bottom edge (top); distribution of the heat fluxes on both $\partial\Omega_1$ and $\partial\Omega_2$ (bottom); $h = L$.

$$u_1\left(x, \frac{h}{2}\right) = 100\sin\frac{\pi x}{L}, \quad 0 \leqslant x \leqslant L, \tag{46b}$$

ARTICLE IN PRESS

L.F. Kallivokas et al. / Comput. Methods Appl. Mech. Engrg. xxx (2004) xxx–xxx 27

$$u_2(0, y) = 0, \quad \text{and} \quad u_2(L, y) = 0, \quad -\frac{h}{2} \leqslant y \leqslant 0,$$

$$\frac{\partial u_2}{\partial y}\left(x, -\frac{h}{2}\right) = 0, \quad 0 \leqslant x \leqslant L, \tag{46c}$$

with $\kappa_1 = 1$ and $\kappa_2 = 2$; for problem (46) the exact solution is given as:

$$u_1(x, y) = \sin\frac{\pi x}{L}\left(\alpha_1 \sinh\frac{\pi y}{L} + \alpha_2 \cosh\frac{\pi y}{L}\right), \quad \text{for } (x, y) \in \Omega_1, \tag{47a}$$

$$u_2(x, y) = \sin\frac{\pi x}{L}\left(\beta_1 \sinh\frac{\pi y}{L} + \beta_2 \cosh\frac{\pi y}{L}\right), \quad \text{for } (x, y) \in \Omega_2, \tag{47b}$$

with

$$\alpha_1 = \frac{200 \sinh\frac{\pi h}{2L}}{2\sinh^2\frac{\pi h}{2L} + \cosh^2\frac{\pi h}{2L}}, \quad \alpha_2 = \frac{100 \cosh\frac{\pi h}{2L}}{2\sinh^2\frac{\pi h}{2L} + \cosh^2\frac{\pi h}{2L}},$$

$$\beta_1 = \tfrac{1}{2}\alpha_1, \quad \beta_2 = \alpha_2. \tag{48}$$

Fig. 17 depicts both exact and approximate solutions over the interface and the bottom edge of subdomain Ω_2. Shown in the same figure are also the heat fluxes on all boundary segments. Notice that now the agreement for the latter is excellent due to the modified discrete variational form (45).

6. Conclusions

In this paper, a symmetric Galerkin boundary element method formulation was presented based on a new variational principle derived for multi-domain interface problems. The key ingredients of this development are:

- A variational principle that allows the systematic treatment of a variety of interfacial problems in mechanics that departs from the current approaches: the coupling of the, so-called, regular and hypersingular boundary element methods is now accomplished within a systematic variational framework.
- The global algebraic equations entail only the primary variables. The normal derivatives and Lagrange multipliers (density of the layers) can be condensed at the subdomain level.
- The treatment of the hypersingular operators: we have used Maue's identity to allow the evaluation of the hypersingular kernels in terms of the weakly-singular single-layer kernels, thereby avoiding the numerical difficulties and special integration schemes typically associated with the numerical evaluation of the hypersingular kernels.
- Subdomain partitioning: we have shown that the contributions of the individual homogeneous subdomains to the resulting algebraic system are independent of the contributions of neighboring subdomains. This allows the ready parallelization of the approach, for the assembly work over each subdomain can be assigned to individual processors. We further remark that the formulation allows partitioning of even homogeneous subdomains, thereby increasing the level of sparsity that the user can introduce, which in turn, allows for fast parallel solutions on appropriate architectures.
- Double- versus single-layer numerical inversion: we have opted to arrive at the variational principle by imposing the normal derivative of the standard integral representation in the modified system Lagrangian via Lagrange multipliers. This choice readily leads to the numerical inversion of a double-layer operator, thus lending increased stability and accuracy to the numerical operations.

ARTICLE IN PRESS

28   *L.F. Kallivokas et al. / Comput. Methods Appl. Mech. Engrg. xxx (2004) xxx–xxx*

- The treatment of corners: we have presented a systematic scheme based on double-node representations of corner nodes that alleviates the observed oscillatory behavior of the normal derivatives at or near corners (due to the multi-valued normals). The treatment of the corners is also cast in variational form and thus maintains the overall symmetry of the system matrices.

A variety of numerical examples were presented to illustrate the methodology.

Acknowledgment

Appendix A. Detailed subdomain matrix expressions

To amplify on the details of the numerical implementation, we provide below all matrix expressions for the matrices defined in (22) and included in the final algebraic system (25). We provide expressions for the generic subdomain (Ω_α). We remark that the contributions of each domain to the overall system matrix, as it can be seen from (25), can be computed independently from other domains, thus lending the overall formulation to ready parallelism.

A.1. Matrix A_α

From the first line of (13) and the definition (22a), there results:

$$\frac{1}{\rho_\alpha} \int_{\partial\Omega_\alpha} \delta u_{\alpha n} u_\alpha \, \mathrm{d}(\partial\Omega_\alpha) = \frac{1}{\rho_\alpha} \int_{\partial\Omega_\alpha} \delta u_{\alpha n}(\boldsymbol{x}) u_\alpha(\boldsymbol{x}) \, \mathrm{d}(\partial\Omega_\alpha(\boldsymbol{x}))$$

$$= \delta\boldsymbol{u}_{\alpha_n}^{\mathrm{T}} \left[\frac{1}{\rho_\alpha} \int_{\partial\Omega_\alpha} \boldsymbol{\psi}_\alpha(\boldsymbol{x}) \boldsymbol{\phi}_\alpha^{\mathrm{T}}(\boldsymbol{x}) \, \mathrm{d}(\partial\Omega_\alpha(\boldsymbol{x})) \right] \boldsymbol{u}_\alpha = \delta\boldsymbol{u}_{\alpha_n}^{\mathrm{T}} \boldsymbol{A}_\alpha \boldsymbol{u}_\alpha, \tag{A.1a}$$

with

$$\boldsymbol{A}_\alpha = \frac{1}{\rho_\alpha} \int_{\partial\Omega_\alpha} \boldsymbol{\psi}_\alpha \boldsymbol{\phi}_\alpha^{\mathrm{T}} \, \mathrm{d}(\partial\Omega_\alpha). \tag{A.1b}$$

A.2. Matrix B_α

From the first line of (13) and the definition (22b), there results:

$$\frac{1}{\rho_\alpha} \int_{\partial\Omega_\alpha} \delta u_{\alpha n} \left(\frac{1}{2} \lambda_\alpha + D_\alpha[\lambda_\alpha] \right) \mathrm{d}(\partial\Omega_\alpha) = \frac{1}{\rho_\alpha} \int_{\partial\Omega_\alpha} \delta u_{\alpha n}(\boldsymbol{x}) \left(\frac{1}{2} \lambda_\alpha(\boldsymbol{x}) + D_\alpha[\lambda_\alpha](\boldsymbol{x}) \right) \mathrm{d}(\partial\Omega_\alpha(\boldsymbol{x}))$$

$$= \frac{1}{\rho_\alpha} \int_{\partial\Omega_\alpha} \delta u_{\alpha n}(\boldsymbol{x}) \left[\frac{1}{2} \lambda_\alpha(\boldsymbol{x}) + \int_{\partial\Omega_\alpha} \lambda_\alpha(\boldsymbol{y}) \frac{\partial G(\boldsymbol{x}, \boldsymbol{y})}{\partial n_{\boldsymbol{y}}} \, \mathrm{d}(\partial\Omega_\alpha(\boldsymbol{y})) \right] \mathrm{d}(\partial\Omega_\alpha(\boldsymbol{x}))$$

$$= \delta\boldsymbol{u}_{\alpha_n}^{\mathrm{T}} \left\{ \frac{1}{\rho_\alpha} \left[\int_{\partial\Omega_\alpha} \frac{1}{2} \boldsymbol{\psi}_\alpha(\boldsymbol{x}) \boldsymbol{\chi}_\alpha^{\mathrm{T}}(\boldsymbol{x}) \, \mathrm{d}(\partial\Omega_\alpha(\boldsymbol{x})) \right. \right.$$

$$\left. \left. + \int_{\partial\Omega_\alpha} \boldsymbol{\psi}_\alpha(\boldsymbol{x}) \left[\int_{\partial\Omega_\alpha} \boldsymbol{\chi}_\alpha^{\mathrm{T}}(\boldsymbol{y}) \frac{\partial G(\boldsymbol{x}, \boldsymbol{y})}{\partial n_{\boldsymbol{y}}} \, \mathrm{d}(\partial\Omega_\alpha(\boldsymbol{y})) \right] \mathrm{d}(\partial\Omega_\alpha(\boldsymbol{x})) \right] \right\} \boldsymbol{\lambda}_\alpha$$

$$= \delta\boldsymbol{u}_{\alpha_n}^{\mathrm{T}} \boldsymbol{B}_\alpha \boldsymbol{\lambda}_\alpha, \tag{A.2a}$$

ARTICLE IN PRESS

L.F. Kallivokas et al. / Comput. Methods Appl. Mech. Engrg. xxx (2004) xxx–xxx 29

with

$$\boldsymbol{B}_{\alpha} = \frac{1}{\rho_{\alpha}} \int_{\partial \Omega_{\alpha}} \boldsymbol{\psi}_{\alpha} \left[\frac{1}{2} \boldsymbol{\chi}_{\alpha}^{T} + D_{\alpha}[\boldsymbol{\chi}_{\alpha}^{T}] \right] d(\partial \Omega_{\alpha}). \tag{A.2b}$$

A.3. Matrix $\boldsymbol{C}_{\alpha}$

From the third line of (13) and the definition (22c), there results:

$$\frac{1}{\rho_{\alpha}} \int_{\partial \Omega_{\alpha}} \delta \lambda_{\alpha} M_{\alpha}[u_{\alpha}] d(\partial \Omega_{\alpha}) = \frac{1}{\rho_{\alpha}} \int_{\partial \Omega_{\alpha}} \delta \lambda_{\alpha}(\boldsymbol{x}) M_{\alpha}[u_{\alpha}](\boldsymbol{x}) d(\partial \Omega_{\alpha}(\boldsymbol{x})). \tag{A.3a}$$

Using Maue's identity (19), (A.3a) becomes (notice that $\boldsymbol{S}_{\alpha}$ below is vector-valued):

$$
\begin{aligned}
\frac{1}{\rho_{\alpha}} \int_{\partial \Omega_{\alpha}} \delta \lambda_{\alpha}(\boldsymbol{x}) M_{\alpha}[u_{\alpha}](\boldsymbol{x}) d(\partial \Omega_{\alpha}(\boldsymbol{x})) &= \frac{k_{\alpha}^{2}}{\rho_{\alpha}} \int_{\partial \Omega_{\alpha}} \boldsymbol{S}_{\alpha}[u_{\alpha}\boldsymbol{n}](\boldsymbol{x}) \cdot (\delta \lambda_{\alpha}\boldsymbol{n})(\boldsymbol{x}) d(\partial \Omega_{\alpha}(\boldsymbol{x})) \\
&\quad - \frac{1}{\rho_{\alpha}} \int_{\partial \Omega_{\alpha}} \boldsymbol{S}_{\alpha}[\boldsymbol{n} \times \overset{y}{\nabla} u_{\alpha}](\boldsymbol{x}) \cdot (\boldsymbol{n} \times \overset{x}{\nabla} \delta \lambda_{\alpha})(\boldsymbol{x}) d(\partial \Omega_{\alpha}(\boldsymbol{x})) \\
&= \delta \boldsymbol{\lambda}_{\alpha}^{T} \left\{ \frac{k_{\alpha}^{2}}{\rho_{\alpha}} \int_{\partial \Omega_{\alpha}} \boldsymbol{\chi}_{\alpha}(\boldsymbol{x}) \left[n_{x}(\boldsymbol{x}) \int_{\partial \Omega_{\alpha}} \boldsymbol{\phi}_{\alpha}^{T}(\boldsymbol{y}) G(\boldsymbol{x},\boldsymbol{y}) n_{x}(\boldsymbol{y}) d(\partial \Omega_{\alpha}(\boldsymbol{y})) \right. \right. \\
&\quad \left. + n_{y}(\boldsymbol{x}) \int_{\partial \Omega_{\alpha}} \boldsymbol{\phi}_{\alpha}^{T}(\boldsymbol{y}) G(\boldsymbol{x},\boldsymbol{y}) n_{y}(\boldsymbol{y}) d(\partial \Omega_{\alpha}(\boldsymbol{y})) \right] d(\partial \Omega_{\alpha}(\boldsymbol{x})) \\
&\quad - \frac{1}{\rho_{\alpha}} \int_{\partial \Omega_{\alpha}} \left[n_{x}(\boldsymbol{x}) \frac{\partial \boldsymbol{\chi}_{\alpha}(\boldsymbol{x})}{\partial y_{x}} - n_{y}(\boldsymbol{x}) \frac{\partial \boldsymbol{\chi}_{\alpha}(\boldsymbol{x})}{\partial x_{x}} \right] \\
&\quad \times \left[\int_{\partial \Omega_{\alpha}} \left[n_{x}(\boldsymbol{y}) \frac{\partial \boldsymbol{\phi}_{\alpha}^{T}(\boldsymbol{y})}{\partial y_{y}} - n_{y}(\boldsymbol{y}) \frac{\partial \boldsymbol{\phi}_{\alpha}^{T}(\boldsymbol{y})}{\partial x_{y}} \right] G(\boldsymbol{x},\boldsymbol{y}) d(\partial \Omega_{\alpha}(\boldsymbol{y})) \right] \\
&\quad \left. \times d(\partial \Omega_{\alpha}(\boldsymbol{x})) \right\} \boldsymbol{u}_{\alpha} = \delta \boldsymbol{\lambda}_{\alpha}^{T} \boldsymbol{C}_{\alpha} \boldsymbol{u}_{\alpha},
\end{aligned}
\tag{A.3b}
$$

where $k_{\alpha}^{2} = \omega^{2}/c_{\alpha}^{2}$, and n_{x}, n_{y} denote the Cartesian components of the normal vector $\boldsymbol{n}$, respectively. Thus:

$$\boldsymbol{C}_{\alpha} = \frac{1}{\rho_{\alpha}} \int_{\partial \Omega_{\alpha}} \boldsymbol{\chi}_{\alpha} M_{\alpha}[\boldsymbol{\phi}_{\alpha}^{T}] d(\partial \Omega_{\alpha}). \tag{A.3c}$$

A.4. Force vector $\boldsymbol{f}_{\alpha}$

From the last line of (13) and the definition (22d), there results:

$$\frac{2}{\rho_{\alpha}} \int_{\Gamma_{\alpha}^{u_{n}}} h_{\alpha} \delta u_{\alpha} d\Gamma_{\alpha}^{u_{n}} = \frac{2}{\rho_{\alpha}} \int_{\Gamma_{\alpha}^{u_{n}}} h_{\alpha}(\boldsymbol{x}) \delta u_{\alpha}(\boldsymbol{x}) d\Gamma_{\alpha}^{u_{n}}(\boldsymbol{x}) = \delta \boldsymbol{u}_{\alpha}^{T} \left[\frac{2}{\rho_{\alpha}} \int_{\Gamma_{\alpha}^{u_{n}}} h_{\alpha}(\boldsymbol{x}) \boldsymbol{\phi}_{\alpha}(\boldsymbol{x}) d\Gamma_{\alpha}^{u_{n}}(\boldsymbol{x}) \right] = \delta \boldsymbol{u}_{\alpha}^{T} \boldsymbol{f}_{\alpha}, \tag{A.4a}$$

with

$$\boldsymbol{f}_{\alpha} = \frac{2}{\rho_{\alpha}} \int_{\Gamma_{\alpha}^{u_{n}}} h_{\alpha} \boldsymbol{\phi}_{\alpha} d\Gamma_{\alpha}^{u_{n}}. \tag{A.4b}$$

References

[1] S. Sirtori, General stress analysis method by means of integral equations and boundary elements, Meccanica 14 (1979) 210–218.

[2] J. Bielak, R.C. MacCamy, An exterior interface problem in two-dimensional elastodynamics, Q. Appl. Math. 41 (1983) 143–159.

[3] M. Bonnet, G. Maier, C. Polizzotto, Symmetric Galerkin boundary element methods, ASME Appl. Mech. Rev. 51 (11) (1998) 669–704.

[4] J. Bielak, R.C. MacCamy, Symmetric finite element and boundary integral coupling methods for fluid–solid interaction, Q. Appl. Math. 49 (1991) 107–119.

[5] J. Bielak, R.C. MacCamy, X. Zeng, Stable coupling method for interface scattering problems by combined integral equations and finite elements, J. Comput. Phys. 119 (1995) 374–384.

[6] X. Zeng, L.F. Kallivokas, J. Bielak, Stable localized symmetric integral equation method for acoustic scattering problems, J. Acoust. Soc. Am. 91 (5) (1992) 2510–2518.

[7] H. Yi, Mixed boundary element methods—theory and applications is solid mechanics, Ph.D. thesis submitted in partial fulfillment for the doctoral degree, Department of Civil and Environmental Engineering, Carnegie Mellon University, 1997.

[8] X. Zeng, L.F. Kallivokas, J. Bielak, A symmetric variational finite element-boundary integral equation coupling methods, Comp. Struct. 46 (6) (1993) 995–1000.

[9] L.J. Gray, G.H. Paulino, Symmetric Galerkin boundary integral formulation for interface and multi-zone problems, Int. J. Num. Methods Engrg. 40 (1997) 3085–3101.

[10] J.B. Layton, S. Ganguly, C. Balakrishna, J.H. Kane, A symmetric Galerkin multi-zone boundary element formulation, Int. J. Num. Methods Engrg. 40 (1997) 2913–2931.

[11] A.W. Maue, Zür Formulierung eines allgemeinen Beugungsproblems durch eine Integralgrleichung, Z. Phys. 126 (1949) 601–618.

[12] G. Krishnasamy, F.J. Rizzo, T.J. Rudolphi, Hypersingular boundary integral equations: their occurrence, interpretation, regularization and computation, in: P.K. Banerjee, S. Kobayashi (Eds.), Developments in Boundary Element Methods—Advanced Dynamic Analysis, vol. 7, Elsevier Applied Science Publishers, 1991, Chapter 7.

[13] X. Zeng, J. Bielak, Exterior stable domain segmentation integral equation method for scattering problems, Int. J. Num. Methods Engrg. 37 (5) (1994) 777–792.

[14] A.J. Burton, G.F. Miller, The application of integral equation methods to the numerical solution of some exterior boundary-value problems, Proc. Royal Soc. London 323 (1971) 201–210.

[15] H. Brakhage, P. Werner, Über das dirichletsche aussenraumproblem für die helmoltzsche schwingungsgleichung, Arch. Math. 16 (1965) 325–329.

[16] L.E. Malvern, Introduction to the Mechanics of a Continuous Medium, Prentice-Hall, Inc., Englewood Cliffs, New Jersey, 1969.

[17] P.K. Banerjee, R. Butterfield, Boundary Element Methods in Engineering Science, McGraw-Hill, Maidenhead, Berkshire, England, 1981.